# Locomotion-dependent auditory gating to the parietal cortex mediates flexible multisensory decisions

Ilsong Choi[1], Seung-Hee Lee[1,2*]

[1]Center for Synaptic Brain Dysfunctions, IBS, Daejeon, 34141, Republic of Korea

[2]Department of Biological Sciences, KAIST, Daejeon, 34141, Republic of Korea

*Correspondence and requests for materials should be addressed to S.-H.L. (e-mail: shlee1@kaist.ac.kr).

## Abstract

Decision-making in mammals is fundamentally based on the integration of several senses. When different sensory inputs guide conflicting outcomes, animals make decisions following the prepotent sensory modality. However, the neural basis of state-dependent flexibility in sensory dominance and multisensory decisions remains obscure. Here, we found that locomotion switched auditory-dominant decisions to visual-dominant ones in mice with audiovisual conflicts. When mice made auditory-dominant decisions, the visual representation in the posterior parietal cortex (PPC) was weakened. Prolonged locomotion restored visual representation in the PPC and induced visually dominant decisions by inhibiting the auditory cortical neurons projecting to the PPC ($AC_{PPC}$). In contrast, it had no effect on the AC projection to the striatum, which mediated auditory decisions. Locomotion activated the AC-projecting secondary motor cortex neurons, which preferentially inhibited the $AC_{PPC}$ neurons. Our findings demonstrate that animals make flexible multisensory decisions by gating auditory afferents to the association cortex depending on locomotor conditions.

## Main

Multisensory integration in the brain, which combines neural information from different sensory modalities, is essential for goal-directed perceptual decisions in an ever-changing environment[1]. Animals can make faster[2,3] and more accurate[4,5] perceptual decisions when they integrate congruent (coherent) multisensory stimuli. On the other hand, animals frequently prioritize one modality over the other in response to conflicting multisensory stimuli and show sensory dominance in their perceptual decisions[6-13]. For instance, when head-fixed mice faced conflicting audiovisual cues (one instructed 'Go' responses while the other instructed 'No-go' responses), they often made decisions following auditory cues[12,13]. This sensory dominance in multisensory decisions cannot be fully explained by a simple additive integration of individual stimuli as explained by a classic Bayesian model[14-16]. Rather, it requires under-weighting one modality more than the other before the integration[10,11,17], potentially via crossmodal inhibition[12,18,19]. Interestingly, the prepotent modality in multisensory decisions not only varies individually but also switches flexibly from trial to trial[10,11,20,21]. Neural underpinnings of this flexibility in multisensory decisions, however, remain largely unexplored.

Perceptual decision-making occurs with sensory representation associated with motor actions across cortical areas[22,23]. The sensory representation is not stable and fluctuates depending on the behavioral states of the animals[24,25]. One key factor affecting the cortical representation of sensory stimuli is the locomotion. Locomotion increases arousal, which amplifies visual gain in the visual cortex (VC)[26-34] but suppresses auditory representations in the auditory cortex (AC)[35,36]. Furthermore, locomotion generates corollary discharge signals copied from motor commands, which also suppress auditory responses in the AC[37,38]. As a result of these representational changes, mice showed better detection of mild visual cues[27] and reduced detection of weak auditory cues[35,39]. Despite this, animals still can identify salient

auditory cues well and perform auditory-dependent perceptual tasks without disruption even during locomotion[40,41]. These reports suggest that, even during locomotion, animals retain salient auditory information in the brain, enabling them to make appropriate auditory decisions. In a multisensory environment containing both visual and auditory stimuli, it is more challenging to determine how locomotion influences the multisensory representation and decision-making processes. Compared to head-fixed mice, freely roaming mice exhibited no differences in unisensory decisions but only shifted prepotent modality from audition to vision during multisensory decisions[13]. However, it is unclear how locomotion modulates neural circuits representing multisensory stimuli in the brain to alter behavioral decisions in mice.

One of the key brain areas that mediate perceptual decision-making is the posterior parietal cortex (PPC)[42-44]. The PPC encodes various task-relevant activities during visual decision-making tasks, conveying information of the category of stimuli[45-48], accumulating sensory evidence[49-51], history of the task variables[48,52], animal's choices[45,48,49,53], and body movements[54]. Furthermore, inactivation of the PPC resulted in a substantial decline in an animal's ability to make visual decisions[45,49,50]. Similar to the visual acitivites, the PPC also showed task-relevant activities during auditory decision-making tasks[48,50,55,56]. Its inactivation, however, did not impair perceptual decisions based on simple auditory feature detection or discrimiation[50,51,56], suggesting that the PPC may work for auditory-dependent decision-making in more complicated context[57,58]. The PPC receives converging inputs from visual, auditory, and somatosensory cortices[59-61] and responds to multisensory stimuli in humans[62], primates[19,63] and rodents[64,65]. However, its role in multisensory decisions is still unclear. PPC inactivation altered multisensory decisions under audiovisual conflicts[12] (but see also[16]), but it did not affect multisensory decisions in coherent conditions[16,50]. These reports suggest that the PPC in multisensory decisions may depend on the task paradigms or multisensory contexts that the animal encounters.

To understand how the PPC is involved in multisensory decisions in animals making perceptual decisions across auditory, visual, and congruent or incongruent audiovisual stimuli, at different behavioral states, we used *in vivo* calcium imaging and optogenetic manipulation techniques in mice performing an audiovisual discrimination task on the treadmill. We discovered that mice flexibly switched the dominant modality from audition to vision during locomotion. The PPC neurons discriminated visual inputs better than auditory inputs, and the visual representation was suppressed when animals made auditory-dominant decisions in audiovisual conflicts. During locomotion, the AC output to the PPC ($AC_{PPC}$) was selectively suppressed, while the AC output to the striatum was maintained. This circuit-specific modulation preserved the visual representation in the PPC and allowed animals to make visually dominant multisensory decisions when animals confronted conflicting audiovisual stimuli during locomotion. The locomotion-induced suppression of $AC_{PPC}$ neurons was mediated by top-down inputs from the secondary motor cortex (M2) to the AC. Our data demonstrate a neural mechanism of flexible multisensory decisions in the face of crossmodal conflicts, which require gating in the auditory-to-parietal circuit according to the animal's behavioral states.

## Results

### Locomotion enhances visually dominant decisions in mice under audiovisual conflicts

To examine state-dependent multisensory decisions in mice, we trained head-fixed mice to discriminate auditory and visual stimuli and make Go/No-go decisions on a non-motorized treadmill (Fig. 1a,b; 10 kHz vs. 5 kHz pure-tones: auditory Go ($A_G$) vs. auditory No-go ($A_{NG}$); vertically vs. horizontally drifting gratings: visual Go ($V_G$) vs. visual No-go ($V_{NG}$)). After mice became experts in discriminating both auditory and visual stimuli at similar correct rates in the stationary (S) state (Fig. 1c), we compared their performance in the moving (M) state (Fig. 1d). During the test, either congruent ($A_GV_G$ or $A_{NG}V_{NG}$) or incongruent ($A_GV_{NG}$ or $A_{NG}V_G$) audiovisual stimuli were randomly presented in a quarter of trials to examine their licking decisions in such multisensory context (Fig. 1e). In the incongruent trials, mice made either auditory-dominant or visual-dominant decisions (Fig. 1e; Methods). Head-fixed mice showed better performance of discriminating congruent audiovisual stimuli compared to auditory- or visual-only stimuli in stationary conditions (Fig. 1f). In moving sessions, the same mice discriminated the unisensory (auditory or visual) stimuli better, often hit the maximum performances, and therefore showed no further improvement in the congruent trials (Fig. 1f). As reported previously[12], stationary mice showed auditory-dominant decisions in response to the incongruent audiovisual stimuli (80.7% auditory dominance rate; Fig. 1g). Interestingly, the moving mice made considerably fewer auditory-dominant decisions (45.6% of the incongruent trials; Fig. 1g).

We further examined the effects of different conditions of locomotion on switching auditory dominance to visual dominance. First, we examined the effect of locomotion duration, as it has been shown that the locomotion-induced changes in cortical states depend on its duration[36,38,66,67]. We compared mice's decisions in the incongruent trials when the stimuli were presented right after locomotion (start-moving, SM) with those when stimuli were presented

after prolonged (> 3s) locomotion (keep-moving, KM). Interestingly, mice showed stronger visual dominance in the keep-moving trials than in the start-moving trials (Fig. 1h). Once they kept moving at a certain speed (> 3cm/s), the pre-stimulus speed did not further affect their decisions in the incongruent trials (Extended Data Fig. 1a). These data indicate that the duration, not the speed, of locomotion is important for switching the dominant modality from audition to vision in mice making decisions under audiovisual conflicts. The unisensory trial types and outcomes of previous trials did not affect the mice's decision in the incongruent trials with or without locomotion (Extended Data Fig. 1b). The level of arousal measured by pupil size was also unrelated to the effect of locomotion on changes in dominant decisions (Extended Data Fig. 1c,d). Therefore, the locomotion duration prior to the stimuli, compared with any other internal factors, is the most critical factor determining which modality becomes dominant.

**Locomotion reduces auditory representation in the PPC**

As the PPC activity is important for mice to make perceptual decisions by integrating auditory and visual inputs[12], we next examined how the PPC excitatory neurons represent task-relevant sensory information in mice performing the audiovisual discrimination task by *in vivo* calcium imaging using a miniature microscope through a prism-combined gradient reflective index (GRIN) lens (Fig. 2a). We first classified neuronal types based on their responses to different sensory stimuli in the unisensory trials accompanied by correct decisions (Fig. 2b,c). To avoid any potent influence of the outcome-related activities, we calculated fluorescence changes during the stimulus period before the outcomes (0 ~ 1s). In the stationary sessions, many of the PPC excitatory neurons were identified as visual-only (41.7%) or multisensory responsive neurons (36.7%), but relatively small portion of them were auditory-only responsive neurons (10.6%) (Fig. 2c). In the moving sessions, the proportion of visual neurons increased (54.7%), and many neurons lost their auditory responses (Fig. 2c,d and Extended

Data Fig. 2a). When we compared the response amplitudes of all PPC neurons, the auditory responses were significantly reduced during locomotion. Still, the visual responses were similar between the stationary and the moving states (Fig. 2d). This finding indicates that locomotion selectively degrades auditory, but not visual responses in the PPC of task-performing mice.

During the task, mice often started to lick within the stimulus period, and the stimulus-evoked activity of the PPC neurons might be mixed with the licking-evoked activities during the stimulus presentation period. To decompose the PPC population activity into specific activities representing sensory stimulus, licking decisions, stimulus-decision interactions, or other independent factors, we used demixed principal component analysis (dPCA)[68]. We fed neural data from the unisensory trials (i.e., $A_G$, $A_{NG}$, $V_G$, $V_{NG}$ with licking or no-licking decisions) for the dPCA (Fig. 2e). We confirmed that the decomposed PPC activity in the stimulus PC axes reliably represented each stimulus information regardless of licking actions after the stimuli (Extended Data Fig. 2b). On the other hand, dPCA properly dissociated decision-relevant activity in the PPC neurons in other axes (Extended Data Fig. 2c,d). Interestingly, the stimulus axis explained the PPC population activity much more than any other axes in both stationary and moving conditions (Fig. 2f and Extended Data Fig. 2e), indicating that the PPC neurons represent sensory information the most strongly during the task.

We next examined how the PPC activity represented auditory and visual Go/No-go stimuli in the stimulus subspace by comparing trial-averaged neuronal trajectories of each unisensory stimulus in the top three PCs (Fig. 2g; mean % explanation by top three stimulus PCs: 62.8%). First, we quantitatively measured the magnitude of sensory representations by calculating the projection distance of each trajectory during the stimulus presentation period (for 1 s after stimulus onset) (Fig. 2g; Methods). Auditory trajectories were much shorter than

visual trajectories and became even shorter as animals made longer locomotion (Fig. 2h). Next, we calculated the Euclidean distance between a pair of trajectories to quantify similarities in the representation of each stimulus type (Fig. 2i and Extended Data Fig. 2f). Auditory Go and No-go trajectories were close to each other and less distinct during locomotion (Fig. 2i). In contrast, visual Go and No-go trajectories were divergent and distinct from each other (Fig. 2i). The visual trajectories also differed from the auditory trajectories (Extended Data Fig. 2f). Finally, to understand the trial-by-trial reliability of unisensory representation in the PPC, we developed a classifier, which predicted the presented stimulus type in the current trial based on the Euclidean distance between the current-trial trajectory and the trial-averaged trajectory (Fig. 2j). Classification accuracies were significantly higher for the visual trials than the auditory trials (Fig. 2k,l). Moreover, accuracies of auditory classification were significantly lower in the moving sessions than in the stationary sessions (Fig. 2l). Collectively, the PPC neurons processed task-relevant visual information more strongly than the auditory information, showing robust visual but weak auditory Go/No-go discrimination. More importantly, locomotion further dampened the auditory representation in the PPC.

**Multisensory representation in the PPC determines the dominant modality for perceptual decisions under audiovisual conflict**

We next examined how the PPC neurons represent multisensory information by projecting their activity into the stimulus subspace during the multisensory trials (Fig. 3a,b; Methods). The neural trajectories representing the congruent multisensory stimuli were very close to the visual trajectories but highly distinct from the auditory trajectories in both stationary and moving conditions (Fig. 3a,b). Euclidean distances, projection distances, and classifier accuracies between the congruent Go and No-go trajectories were not different from those between the visual Go and No-go trajectories regardless of locomotion conditions

(Extended Data Fig. 3a-d). These findings suggest that PPC neurons represent congruent multisensory inputs in a similar way that they do visual stimuli.

By projecting PPC activity trajectories during the incongruent multisensory trials, we found that PPC neurons represented the same stimulus condition ($A_{NG}V_{G}$ or $A_{G}V_{NG}$) differently depending on the impending decisions of mice (Fig. 3c; auditory dominance in grey trajectories vs. visual dominance in black trajectories). We first found that the projection and the Euclidean distances of the trajectories for the auditory-dominant incongruent trials were smaller than those for the visual-dominant trials (Extended Data Fig. 3e,f). Furthermore, the trajectories representing the incongruent stimuli were nearly identical to those representing visual stimuli when mice made visually dominant decisions (Fig. 3d and Extended Data Fig. 3g). When mice made auditory-dominant decisions, however, the neural trajectories for the incongruent stimuli diverged from the visual trajectories, becoming closer to but still separate from the auditory trajectories (Fig. 3d and Extended Data Fig. 3g).

We next classified the incongruent trials individually by calculating the Euclidean distance between the single-trial trajectory and the mean trajectories of the four types of multisensory trials and found that the classification accuracy was significantly higher in the stimulus subspace than in other subspaces (Extended Data Fig. 3h). Therefore, the sensory representation in the PPC is the most critical factor determining the multisensory decisions of mice in the audiovisual conflict during the task. We further developed another classifier by setting the boundary of the visual trajectories based on their trial-by-trial variations and classified the individual incongruent trajectories as visually dominant ones if they were within the boundary of the visual trajectories (Fig. 3e). Using this, we successfully classified the dominant modality across the incongruent trials (Fig. 3f). Collectively, if the PPC neurons dominantly represented visual information in the incongruent audiovisual stimuli, mice showed visually dominant decisions in the incongruent trials. Conversely, if the visually dominant

representation weakened in the PPC, mice made auditory-dominant decisions in response to the incongruent stimuli.

To understand if the stimulus representation in the PPC changes with locomotion, we calculated the divergence between the incongruent multisensory trajectory and the visual trajectory at different locomotion states (Fig. 3g). The two trajectories were closer as the animal made longer locomotion, and this was correlated with the decrease in auditory dominance rates in the animal's multisensory decisions (Fig. 3g). In correlation with such changes, visually responsive neurons showed stronger suppression in stationary conditions than in moving conditions, but only in the incongruent trials (Fig. 3h). In contrast, auditory-responsive neurons showed significantly low auditory responses during locomotion across all types of trials (Fig. 3h). Therefore, locomotion increased the likelihood of maintaining the visual representation while reducing the auditory representation of the incongruent multisensory stimuli in the PPC and caused mice to make visually dominant multisensory decisions.

**Locomotion selectively suppresses auditory cortical outputs to the parietal cortex but not to the striatum**

The robust reduction of auditory representation in the PPC during locomotion might be due to direct suppression of the auditory neurons in the PPC or indirect suppression of the AC output neurons that project to the PPC (i.e. $AC_{PPC}$ neurons). To examine which case it was, we measured the spontaneous activity changes in the PPC auditory-responsive neurons during locomotion. Neither the locomotion onset nor offset induced significant suppression in their activities (Extended Data Fig. 4a-d). Therefore, the suppression of the auditory responses in the PPC during locomotion is unlikely to result from direct inhibition of the PPC auditory neurons. Instead, it might be due to the reduction of bottom-up auditory inputs to the PPC.

To examine this, we first traced the $AC_{PPC}$ neurons by injecting the retrograde adeno-associated viruses (AAVrg) encoding tdTomato into the PPC (Fig. 4a). We co-traced the AC neurons that project to the posterior striatum ($AC_{STR}$), which are known to play a critical role in the auditory decision-making of mice[69-72], by injecting the AAVrg encoding eGFP into the striatum (Fig. 4a). $AC_{PPC}$ neurons were mostly found in the anterior and dorsal AC (AuD), whereas $AC_{STR}$ neurons were found across the anterior-to-posterior and dorsal-to-ventral AC (Fig. 4b,c). Only 7% of the traced neurons in the AC were co-labeled, suggesting that the $AC_{PPC}$ and the $AC_{STR}$ neurons are distinct and non-overlapping neuronal populations in the AC (Fig. 4d).

We next measured the activity of $AC_{PPC}$ and $AC_{STR}$ neurons in mice running on the treadmill (Fig. 4e,k). When animals started to move, the spontaneous activity of $AC_{PPC}$ neurons was significantly reduced, and their calcium activities and locomotion onset speeds were negatively correlated (Fig. 4f). $AC_{PPC}$ neurons were liberated from the inhibition at locomotion offsets (Fig. 4g). Unlike the $AC_{PPC}$ neurons, $AC_{STR}$ neurons did not exhibit any activity changes at the onset or offset of locomotion (Fig. 4l,m). These results demonstrate that locomotion suppressed $AC_{PPC}$ neurons directly and selectively without inhibiting $AC_{STR}$ neurons.

**Locomotion reduces task-relevant auditory representation in the $AC_{PPC}$ neurons**

We next examined the stimulus-evoked activities of $AC_{PPC}$ and $AC_{STR}$ neurons during the task. Both $AC_{PPC}$ and $AC_{STR}$ neurons showed significant auditory responses but no profound visual responses during the task (Extended Data Fig. 5a-c and Extended Data Fig. 6a-c). Prolonged locomotion suppressed the auditory responses of the $AC_{PPC}$ neurons (Extended Data Fig. 5c). In the incongruent trials, $AC_{PPC}$ neurons showed strong responses when animals made auditory-dominant decisions but significantly weak responses during visually-dominant decisions (Fig. 4h,i). Locomotion-induced suppression of the $AC_{PPC}$

neurons was correlated with reduced auditory dominance in multisensory decisions of mice (Fig. 4j). However, there was no such suppression in the $AC_{STR}$ neurons during locomotion, and the population of $AC_{STR}$ neurons showed auditory responses at similar levels across the trials independent of locomotion conditions and dominant modalities (Fig. 4n-p and Extended Data Fig. 6c).

We further analyzed AC population activity using the dPCA. As shown in the PPC neurons, the stimulus axis explained the activities of both AC subpopulations more strongly than other task-relevant axes (data not shown). During locomotion, the auditory trajectories significantly shrank only in the $AC_{PPC}$ neurons (Extended Data Fig. 5d-f), but not in the $AC_{STR}$ neurons (Extended Data Fig. 6d-f). Furthermore, only $AC_{PPC}$ neurons showed decreased classification accuracies for the auditory stimuli during locomotion (Extended Data Fig. 5g and Extended Data Fig. 6g). During the incongruent trials, the response amplitudes and the neural trajectories of the $AC_{PPC}$ neurons were significantly smaller in the visual-dominant trials than in the auditory-dominant trials (Extended Data Fig. 5h-j). In contrast, $AC_{STR}$ neurons showed consistent responses to the incongruent stimuli regardless of dominant modalities (Extended Data Fig. 6h-j). These data indicate that locomotion suppressed the $AC_{PPC}$ neurons more than $AC_{STR}$ neurons, and this selective suppression switched mice to make visually dominant decisions in the incongruent trials. In contrast to the vulnerability of the $AC_{PPC}$ neurons, $AC_{STR}$ neurons were unaffected by locomotion, suggesting that the $AC_{STR}$ neurons reliably encode auditory information even during locomotion and are unrelated to multisensory decisions influenced by the locomotion.

**Optogenetic double dissociation reveals distinct roles of the AC subpopulations in perceptual decisions during the audiovisual discrimination task**

We wondered whether the two distinct AC outputs, $AC_{PPC}$ and $AC_{STR}$, play distinct functional roles during the audiovisual discrimination task. We first examined whether the activity in the $AC_{PPC}$ neurons was required for auditory dominance in multisensory decisions of mice in the incongruent trials. We expressed halorhodopsin (eNpHR3.0) in $AC_{PPC}$ neurons and optogenetically inhibited them in task-performing mice (Fig. 5a). Optogenetic inhibition of the $AC_{PPC}$ neurons did not affect the mice's decisions in the auditory, visual, and congruent audiovisual trials (Fig. 5b,d). However, it caused a significant reduction in auditory-dominant decisions in stationary mice (Fig. 5c,e).

We next examined the role of $AC_{STR}$ neurons during the task by optogenetic inhibition of those neurons (Fig. 5f). Similar to previous studies[69,70], inhibition of the $AC_{STR}$ neurons significantly hampered auditory discrimination in stationary mice (Fig. 5g,i). At the same time, it caused only a mild reduction of auditory-dominant decisions in the incongruent trials (Fig, 5h,j). Our findings indicate that the AC-to-STR circuit is important for perceptual decisions in auditory-only conditions. In contrast, the AC-to-PPC circuit is necessary for animals to make auditory-dominant decisions under audiovisual conflicts.

**Motor cortical projection to the AC suppresses $AC_{PPC}$ neurons during locomotion**

Previous research reported that the neural projection from the M2 to the AC suppressed auditory responses of AC neurons[37,38]. Our data further showed that locomotion suppressed the $AC_{PPC}$ neurons but not the $AC_{STR}$ neurons. To examine if the M2 mediates this selective suppression of the $AC_{PPC}$ neurons, we first anatomically mapped the spread of fluorescence-labeled M2 axons in the AC (Fig. 6a). Similar to the previous report[37], M2 axons primarily innervated the superficial or deep layers of the AuD (Fig. 6b). When we compared the M2 axon distribution with the distributions of the $AC_{PPC}$ and the $AC_{STR}$ neurons across AC areas, M2 axons were localized at a similar location where the $AC_{PPC}$ neurons were found (Fig. 6c). On

the other hand, majority number of the $AC_{STR}$ neurons did not overlap well with the M2 axons (Fig. 6c). This anatomical feature of the overlap between the M2 axons and the $AC_{PPC}$ neurons in the AuD suggests potential modulation of the $AC_{PPC}$ neurons by the M2 during locomotion.

We next investigated whether M2 neurons that project to the AC were activated during locomotion. We measured the calcium activity of the AC-projecting M2 neurons ($M2_{AC}$) in mice running on the treadmill (Fig. 6d). $M2_{AC}$ neurons showed robust activation at the locomotion onset (Fig. 6e), and the calcium activities of these neurons were significantly higher during the later period of locomotion than those right after the locomotion onset (Fig. 6f). This result indicates that the M2 neurons copied and delivered the locomotion onset signal to the AC. We then examined whether this M2 activity suppressed the $AC_{PPC}$ neurons directly without affecting the $AC_{STR}$ neurons. Using the miniature fluorescence microscope conjugated with optogenetic manipulation system (nVoke), we activated the M2 axon terminals in the AC while imaging the calcium activity in the AC subpopulations (Fig. 6g). Optogenetic activation of M2 axons significantly dampened auditory responses of the $AC_{PPC}$ neurons (Fig. 6h,i). In contrast, the $AC_{STR}$ neurons were unaffected by the M2 axon activation, showing consistent auditory responses during the M2 axon activation (Fig. 6j,k). Lastly, we optogenetically inhibited the M2 axon terminals in the AC in mice performing the task (Fig. 6l) and found that it did not alter the animal's decisions in the unisensory or congruent trials (Fig. 6m). However, it significantly enhanced auditory dominance in the incongruent trials during locomotion (Fig. 6n). These results strongly support the idea that locomotion raises activity of the M2-to-AC circuit[38], and we further found that the locomotion-induced activation of this cortical circuit selectively inhibits the AC outputs to the PPC. Consequently, PPC activity is dominated by visual information during locomotion, leading to more visually dominant decisions in mice facing audiovisual conflicts (Fig. 6o).

## Discussions

In this study, we newly identified the neural mechanism for flexible multisensory decisions in mice under audiovisual conflicts. The auditory cortical outputs to the parietal cortex inhibited visual representation in the PPC and caused auditory-dominant decisions. These output neurons were suppressed by locomotion, and such suppression caused animals make more visually dominant decisions. However, locomotion did not suppress the auditory outputs to the STR, allowing animals to make precise auditory decisions even during locomotion. Our findings demonstrate that top-down projection from the M2 to the AC gates auditory outputs to the higher association cortex specifically and shapes flexible decisions under audiovisual conflicts without disrupting perceptual decisions in a simple auditory environment in behaving animals.

### Locomotion and multisensory decision-making

As all animals naturally locomote while collecting sensory information in the environment to make decisions, understanding the role of locomotion in perceptual decision-making is ethologically critical. More recently, using small animals like mice, perceptual experiments for head-fixed mice on the treadmill were devised[31]. Using this system, previous studies have examined the effects of locomotion on the simple detection of a single type of sensory cue[27,35,39], but the effect of locomotion on the discrimination of different modality inputs and multisensory decision-making has never been tested. Our study designed a new behavioral paradigm to measure perceptual decision-making performances in the unisensory (visual or auditory) and multisensory (congruent or incongruent) conditions at different locomotion states within one session in the same animal. We found that locomotion can improve both visual and auditory perceptual decisions after discrimination of salient stimuli in the same animal. This might be because of the increased arousal during locomotion, which can enhance visual and auditory discriminability in the sensory cortices[34,73].

We further found that locomotion can switch multisensory decisions from auditory-dominant to visual-dominant ones in mice. The effect of locomotion on multisensory perception and decision has never been examined before. Our findings demonstrate that the dominant modality can be flexibly switched from audition to vision depending on the locomotion states. Sensory dominance in multisensory decisions can be beneficial for animals to make rapid perceptual decisions[74], which is critical for the survival of animals in a complicated world. Depending on the task design, specific sensory modality information provides more reliable information than other modalities during multisensory integration[74]. A more reliable sensory modality can provide a stronger effect on multisensory decisions in animals performing the task. For example, visual information is more critical for animals to discriminate spatial locations of the multisensory stimuli[9], while auditory information is more important for temporal discrimination of the stimuli[75]. Our study suggests that the locomotion condition of an animal can flexibly switch the appropriate modality even during the same task. The determination of the dominant modality has been explained by Bayesian models, which explain the optimal strategy of re-weighting different sensory inputs based on their reliability (or variance)[10,11,14]. Our data further suggest that the locomotion generates a self-initiated internal signal that can change the relative weights of the auditory inputs compared to the visual inputs by lowering reliability of the auditory information in the parietal cortex, where the dominant modality is determined.

**Locomotion-induced circuit-specific suppression of auditory outputs during multisensory decisions**

Locomotion increases corollary discharge signals in the M2, potentially degrading auditory representations in the AC[38,76]. We further found that locomotion-evoked suppression of auditory responses only happened in the auditory-to-parietal projection, without impairing

auditory responses in the auditory-to-striatal projection (Fig. 4 and Extended Data Fig. 5,6). Therefore, corollary discharge signals evoked by locomotion weaken a specific auditory flow from the AC to the higher association cortex. This caused animals to rely less on auditory stimuli for their decisions under crossmodal conflicts. Future studies are required to understand how the top-down inhibitory synaptic connection from the M2 is only formed in the $AC_{PPC}$ but not in the $AC_{STR}$ neurons.

Using circuit-specific calcium-imaging and optogenetic experiments, we found that $AC_{PPC}$ neurons were mainly necessary for auditory-dominant decisions in the audiovisual conflicts, but $AC_{STR}$ neurons were critical for auditory-based discrimination. The divided roles of the AC outputs may allow the mammalian brain to take advantage of preserved auditory processing during locomotion to make auditory-dependent decisions errorlessly while switching dominant modality in multisensory decisions only when sensory inputs make conflicts.

Similar to the locomotion effect on the auditory system, saccadic eye movement suppresses visual representation in the lower visual areas of the animal[77,78]. However, we found that locomotion did not weaken the visual representation in the PPC (Fig. 2), although some individual neurons reshaped (either increased or decreased) their visual responsiveness during locomotion. It is also known that locomotion evokes strong cholinergic activation, which enhances visual representation in the VC[29]. Future studies are required to know whether inhibitory modulation by the M2 activation during locomotion is specific in the AC and how the locomotion-evoked sensory degradation is compensated by the enhanced arousal in the visual system.

**Functional role of PPC in perceptual decision making**

Similar to the previous research[51], we found the PPC excitatory neurons represent visual information more reliably than the auditory information during the task. Our data further showed that strong auditory inputs to the PPC can disrupt the visual representation, facilitating auditory-dominant multisensory decisions. Interestingly, the PPC excitatory neurons could not discriminate auditory Go/No-go information during the auditory-based decisions, indicating that the PPC itself is not involved in auditory decision-making. Rather, its function as a higher visual area is integrating auditory inputs to determine the visual weights for the multisensory decisions. We also found that the AC output to the STR, which is important for auditory decision-making, showed stable auditory representation even in the visually dominant decisions (Fig. 4 and Extended Data Fig. 6). Future studies are required to fully understand whether the strong visual representation in the PPC is only required or whether any downstream areas of the $AC_{STR}$ neurons need to be further suppressed to switch the auditory-dominant decisions to the visually dominant ones.

Our data also indicate that the suppression of visual responses in the PPC only occurs in the incongruent trials (not congruent trials) when animals make auditory-dominant decisions (Fig. 3h). One potential explanation for this congruency-dependent crossmodal suppression would be an antagonistic selectivity between Go and No-go stimuli in auditory-to-visual inhibitory circuits. Supporting this idea, opponent inhibition between choice-selective neurons was recently found in the PPC[79]. Our previous report showed that pavalbumin-expressing ($PV^+$) neurons in the PPC strongly received AC inputs and mediated auditory-dominant behaviors[12]. Future studies are required to examine whether the selectivity of inhibitory neurons emerges with learning in these inhibitory neurons in the PPC. Similar to the role of the mouse PPC exerting crossmodal inhibition, the human prefrontal cotex[80] and the superior temporal sulcus[17,81] also showed multisensory depression in resolution of conflicting audiovisual speech stimuli. Therefore, multisensory depression might happen across

association areas when animals face multisensory conflicts, and our study demonstrates how the brain flexibly controls the resolution of multisensory conflicts by gating bottom-up inputs.

Our task design used Go/No-go decisions of animals in each trial, which are binary reports and hard to represent differences in the level of perceptual decisions as a continuum across trials. Furthermore, the population of the PPC neurons did not show any significant enhancement in the representation of the congruent audiovisual stimuli compared to the visual-only stimuli. Therefore, other areas, instead of the PPC, may integrate auditory inputs additively and represent congruent multisensory information more reliably to improve animals' perceptual discriminability in the congruent trials. One potential downstream area might be the frontal motor cortex, as the additive multisensory integration[16], as well as the auditory-based decision-making, require M2 activity[82]. Future studies are required to determine whether these circuits are further recruited beyond the PPC to make flexible multisensory decisions in mice.

**Acknowledgements**

We thank Dr. Alex C. Kwan for helpful discussions of imaging data analysis. We thank Dr. Jae-Hyun Kim for helping pupil data analysis.This work was supported by grants to S.-H.L. from the National Research Foundation of Korea funded by the Ministry of Science & ICT (NRF-2021R1A2C3012159) and the Institute for Basic Science (IBS-R002-A2).

**Author Contributions**

I.C. and S.-H.L. conceived and designed all experiments and wrote the manuscript. I.C. performed all experiments and analyzed the data.

**Competing interest declaration**

The authors declare no competing interests.

**Data availability**

All the representative data that support the findings will be publicly available on GitHub. Further requests for the data used in this study can be directed to the corresponding author (shlee1@kaist.ac.kr)

**Code availability**

All custom MATLAB codes to analyze and visualize the data will be publicly available on GitHub.

## Methods

### Animals and surgery

*Animals*

All experimental procedures were approved by the KAIST Institutional Animal Care and Use Committee (IACUC-18-100, IACUC-18-235). Both male and female mice (P45-P150) were used in this study. Animals were maintained *ad libitum* under light (8 am-8 pm) and dark cycle (8 pm-8 am) conditions and housed under single animal per cage conditions from the start until the last day of the experiment. We used C57BL/6J wild-type (WT) mice, B6.Cg-Tg(Camk2a-cre)T29-1Stl/J mice (CaMKIIα-Cre, stock no. 005359, Jackson Laboratory), and Ai162 mice (stock no. 031562, Jackson Laboratory).

*Common procedure of animal surgery*

Adult mice (P45-P80) were anesthetized with isoflurane (1.5%–2% in oxygen) and fixed their head on the stereotaxic apparatus. The body temperature was monitored and maintained at 37°C using a heating pad connected to a body temperature sensor. The scalp was alternately sterilized three times with 70% ethanol and povidone-iodine solution. After the sterilization of the scalp, surgical scissors was used to cut the scalp according to the midline (for virus injection) or remove a portion of the scalp (for the implantation of head plates, GRIN lens, and optic fiber). Periodsteum above the skull was removed, and povidone-iodine solution was used to sanitize the exposed skull and incision. Lastly, we cleaned the exposed skull with sterilized phosphate-buffered saline (PBS).

*Virus injection for retrograde tracing*

For the retrograde tracing of the AC neurons that project to the PPC and the STR, we injected 0.5 μl of retrograde AAV expressing tdTomato (AAVrg-CAG-tdTomato, Addgene)

and 0.5 μl of retrograde AAV expressing GFP (AAVrg-CAG-GFP, Addgene) into the target areas respectively. After 2~3 weeks from the injections, we perfused mice to collect the brain samples for histology.

*Head plate implantation surgery for mouse head-fixation*

To implant a stainless steel head-plate on the mouse head, three miniature stainless steel screws (J.I. Morris) were implanted into the exposed skull using cyanoacrylate glue (Loctite super glue 401, Henkel). A customized stainless steel head-plate was attached on the skull with the cyanoacrylate glue, and the between the skull and head-plate was filled by dental acrylic (Ortho-Jet, Lang Dental).

*Surgical procedures for in vivo calcium imaging*

To express GCaMP6s in the target neurons, we made a small craniotomy (diameter ~0.5 mm) above the targeted location. To conduct *in vivo* calcium imaging at the PPC, we injected ~0.5 μl of Cre-recombinase dependent adeno-associated virus (AAV) expressing GCaMP6s (AAV5-Syn-Flex-GCaMP6s-WPRE-SV40, UPENN) into a site 0.2mm posterior from the right PPC (bregma -2.15mm, lateral -1.6mm, depth -0.35mm) of CaMKIIα-Cre mice using a thin pulled glass pipette (20~25μm of tip diameter, item no. 504949, WPI) installed in a Nanoliter 2010 injector (WPI) at a speed of 24nl/min. For *in vivo* calcium imaging of $AC_{PPC}$ neurons, we injected ~0.5 μl of retrograde AAV expressing GCaMP6s (AAVrg-hSyn1-GCaMP6s-P2A-nls-dTomato, Addgene) into the right PPC (bregma -1.95mm, lateral -1.6mm, depth -0.35mm) of the WT mice. For *in vivo* calcium imaging of $AC_{STR}$ neurons, we injected ~0.5 μl of retrograde AAV expressing GCaMP6s (AAVrg-hSyn1-GCaMP6s-P2A-nls-dTomato, Addgene) into the right STR (bregma -1.5mm, lateral -3.45mm, depth -2.8mm) of the WT mice. For *in vivo* calcium imaging of AC-projecting M2 neurons, we injected ~0.5 μl

of retrograde AAV expressing Cre-recombinase (AAVrg-hSyn-Cre, Addgene) into the right AC (bregma -2.5mm, lateral 4.2mm, depth -0.8mm) of the Ai162 mice. For *in vivo* calcium imaging of AC neruons with optogenetic of M2 axons with nVoke system (Inscopix), we injected ~0.5 μl of retrograde AAV expressing Cre recombinase into the right PPC or STR, and injected ~0.5 μl of AAV-hSyn-ChrimsonR-tdTomato (Addgene) into the right M2 at two anterior-posterior (AP) coordinates (bregma +1.0mm & +1.7mm, lateral -0.75mm, depth -0.6mm) of Ai162 mice. After the injection, the incision was sutured with a stitching fiber and disinfected with a povidone-iodine solution.

After 10-14 days from the virus injection, gradient reflective index (GRIN) lens implantation surgery was conducted as previously demonstrated[83]. Mice received subcutaneously injection of carprofen (5mg/Kg) and dexamethasone (5mg/Kg) 1 hour before the surgery. After anesthetization of a mouse, a $1mm^2$ of square-shaped craniotomy was made on the skull above the area of implantation. A prism-attached GRIN lens (1050-004601 or 1050-004606, Inscopix) was inserted 0.2mm away from the imaging area, where we made a small linear incision of the cortical surface using a surgical knife (10055-12, Fine Science Tools) coupled to the stereotaxic apparatus. The GRIN lens was gently inserted (-0.1mm/20 s, depth -0.8mm for the PPC and the VC; -1.4mm for the AC; 1.1mm for the M2) in different directions of the image plane based on the target areas (PPC and AC: along the medial-lateral axis; VC and M2: along the anterior-posterior axis). The exposed brain tissue between the GRIN lens and skull was covered with Kwik-Sil (WPI), and the inserted GRIN lens was secured by applying Super-Bond (Super-Bond C&B Kit, Sun Medical Co.) and the cyanoacrylate glue over the cured Kwik-Sil layer and connected skull. Mice were then implanted with the head plates. Mice were subcutaneously injected with carprofen and dexamethasone for three days following surgery. The field of view of each mouse was examined on a regular basis, and if we detected obvious neuronal activity, we fastened a

baseplate (1050-004638, Inscopix) atop the GRIN lens using dental acrylic. To protect the lens from dirt, the baseplate was covered with a baseplate cover (1050-004639, Inscopix).

*Surgical procedure for optogenetic manipulation during behavior task*

For optogenetic inhibition of projection-specific AC neurons, we bilaterally injected retrograde AAV expressing Cre-recombinase (AAVrg-hSyn-Cre-WPRE-hGH, Addgene) into the right PPC or bilateral STR (0.5 μl per each site) and 0.5 μl of Cre-recombinase-dependent AAV expressing eNpHR3.0-mCherry (AAV2-EF1a-DIO-eNpHR3.0-mCherry, UNC Vector Core) into the AC. For optogenetic inhibition of the M2-to-AC circuit, we injected the excitatory-neuron-specific AAV expressing ChR2-eYFP (AAV2-CAMKIIa-ChR2-EYFP, UNC Vector Core) or the AAV expressing eNpHR3.0-eYFP in neurons (AAV2-hSyn-eNpHR3.0-eYFP, UNC Vector Core) into the right M2 at two anterior-posterior (AP) coordinates of WT mice (0.5 μl per each coordinate). After the injection, mice were further implanted with the head plates. Mice had 14 days of viral expression before starting water restriction for the behavioral experiment. When mice were trained and ready for the manipulation experiment (see Methods; **Behaviors**), we provided mice with sufficient water for 2 days and implanted optic fiber on target sites for the laser light delivery. Mice were anesthetized with 1.5%-2% isoflurane, and a 0.5mm-diameter craniotomy was made on the right AC. An optic fiber with a 200μm diameter was implanted into the AC (0.6mm depth) and glued with Kwik-Sil and cyanoacrylate glue. For the $AC_{STR}$ inhibition (Fig. 5f-j), we implanted optic fibers into the AC bilaterally. We recovered mice for three days after the surgery and restarted the water restriction and behavioral training.

**Behaviors**

*Hardware setups for behavior experiments*

Visual stimuli were generated with a custom MATLAB code. A gamma-corrected LCD monitor (12cm x 9cm; minimal luminance: 0 lux; maximal luminance: 120 lux; refresh rate: 60Hz) was placed 10 cm away from the left eye of mice at a 45° angle from the rostral-caudal axis. For the binocular visual stimulation task, we put another monitor in front of the right eye of mice as we put on the left side. Full-field drifting gratings (100% contrast, 2 Hz temporal resolution, 0.04 cycles/° spatial resolution, 60Hz refresh rate) were used for the visual discrimination task in two directions (rightward for Go; upward for No-go). Auditory stimuli were generated with a custom MATLAB code (sampling rate 119,000Hz, 16bit). A speaker (#60108, Avisoft) was placed 10cm away from the left ear of the mice. Pure tones with different frequencies (10kHz for Go, 5kHz for No-go in the main task) were used for the auditory discrimination task. All sound stimuli were calibrated to have a 76dB sound pressure level (SPL) at the left ear of mice.

Licking behavior of task-performing mice was detected by a custom-made lickometer. We delivered water reward and air punishment via solenoid valves (EV-2-24, Clippard). All the hardware components were operated and controlled by Presentation (Neurobehavioral Systems) with USB data acquisition devices (USB-201, Measurement Computing). An optical mouse (G100s, Logitech) was placed beside a spinning disk of the treadmill. The rotation of the disk during locomotion was converted to digitalized signals by the optical mouse, and real-time locomotion speed was calculated by a customized LabView code (sampling rate: 40Hz). If the speed exceeded the locomotion threshold (3 cm/s), a 5V-digital signal was sent to the Presentation software in real time through a USB data acquisition device (USB-6001, National Instruments) to present sensory stimuli during locomotion.

*Behavioral training and multisensory discrimination experiments*

Mice underwent water restriction (~1 ml of water per day) throughout the behavioral experiment. The weight of mice under the water restriction was monitored throughout the experiments and maintained at more than 75% of the initial body weight before the water restriction. We calculated the hit rate, FA rate, auditory dominance rate, and correct rate as follows:

*Correct rate (%) = (#Hit trials + #CR trials) / #Total trials X 100*

*Hit rate (%) = #Hit trials / (#Hit trials + #Miss trials) X 100*

*FA rate (%) = #FA trials / (#CR trials + #FA trials) X 100*

*Auditory dominance rate (%) =*

*(#$A_G V_{NG}$→A trials + #$A_{NG} V_G$→A trials) / #Incongruent trials X 100*

*Auditory dominance rate of $A_G V_{NG}$ trials (%) = #$A_G V_{NG}$→A trials / #$A_G V_{NG}$ trials X 100*

*Auditory dominance rate of $V_G A_{NG}$ trials (%) = #$A_{NG} V_G$→A trials / #$A_{NG} V_G$ trials X 100*

All mice were trained and tested through the following five steps:

1) reward conditioning, 2) stimulus conditioning, 3) audiovisual discrimination training, 4) treadmill habituation; 5) audiovisual integration test

1) Reward conditioning: water-restricted mice received 0.8μl of water reward whenever they licked the water port. If mice did not show any spontaneous licking behavior within the first 3 minutes after the beginning of a session, we manually delivered water through the water port until mice started to lick the water port. If mice got more than 0.8ml of total water reward (> 1000 licks) within the first 20 minutes without manual water delivery, mice were moved to the second step in the next session.

2) Stimulus conditioning: auditory go stimulus, visual go stimulus, and no stimulation trials were pseudo-randomly presented in the proportion of 1:1:2. If mice licked the water port during 2 s of response window after the stimulus offset, 1μl of water reward and 2 s of reward consumption time were presented (hit). If mice did not lick the water port until the offset of the

response window (miss), 1μl of water reward was delivered at the end of the response window to encourage learning. If mice licked the water port during the no stimulation trial (false-alarm, FA), 6 s of additional time-out period was given. We gave 4 seconds extra time for the inter-trial interval before beginning the next trial. Task sessions automatically ended when mice consecutively missed 30 auditory- or visual-Go stimuli. When mice showed more than 80% hit rates for visual and auditory go stimuli, mice were moved on to the third step in the next session.

3) Audiovisual discrimination training: 4 types of stimuli (auditory Go, auditory No-go, visual Go, visual No-go) were pseudo-randomly presented in equal proportion. There was no water reward in the miss trials, and 400ms of air puff punishment was delivered to the right cheek of mice with the time-out period (6 s) in the FA trials. Task sessions automatically ended when mice consecutively missed 10 auditory- or visual-Go stimuli. If mice achieved correct rates higher than 80% for both auditory and visual discrimination, we considered that the mice learned the discrimination tasks.

4) Treadmill habituation: We first habituated mice to run on the treadmill during the task by presenting the same auditory and visual stimuli when mice ran faster than a speed threshold (3cm/s). If mice reached an expert level of discrimination (> 80% of correct rates) while showing enough locomotion activity (> 400 trials within 1 hour), mice consecutively performed the task in the stationary block on the immobilized treadmill and in the moving block on the free-rotating treadmill during a single day in random order. If mice showed an expert level of performance in both conditions, they were moved on to the final step. We conducted optic fiber implantation surgery for the optogenetic manipulation experiments when animals passed this step.

5) Audiovisual integration test: auditory, visual, congruent ($A_GV_G$, $A_{NG}V_{NG}$), and incongruent ($A_GV_{NG}$, $A_{NG}V_G$) stimuli were pseudo-randomly presented in the proportion of 3:3:1:1 or 3:3:2:2 for main behavioral test. 3:3:2:2 (for optogenetic experiments and *in vivo* calcium

imaging) or 3:3:1:3 (*in vivo* calcium imaging) ratio was used for the audiovisual integration test to reserve enough trial numbers. There was no water reward and air puff punishment in the incongruent trials. Mice conducted both stationary and moving blocks in random order on a single day except for *in vivo* calcium imaging experiments (See the section on *in vivo* calcium imaging experiments).

In moving sessions, we divided trials into two categories: start-moving trials and keep-moving trials. If the average speed before the stimulus onset (-3 ~ -1.5 s) exceeded the speed threshold (> 3 cm/s), that trial was classified as keep-moving. To evaluate the correlation between locomotion speed and auditory dominance (Extended Data Fig. 1a**)**, we categorized keep-moving incongruent trials according to mean locomotion speed (3 ~ 9 cm/s, 9 ~ 15 cm/s, and higher than 15 cm/s) before the stimulus onset (-1 ~ 0 s). We next determined the auditory dominance rate for each category. To analyze the correlation between trial history and auditory dominance (Extended Data Fig. 1b), we collected and calculated the auditory dominance rates for the following trial sequences: 1) $V_G$ or $A_{NG}$ trial followed by $A_{NG}V_G$ trial, and 2) $A_G$ or $V_{NG}$ followed by $A_GV_{NG}$ trial during the moving sessions. We then estimated the auditory dominance rate based on the modality of the previous trial. To find the relationship between auditory dominance rate and pupil size, we averaged the maximum-normalized pupil size before the stimulus onset (-1 ~ 0 s) during moving sessions. We then calculated the average value of each variable according to the dominant modality.

*Optogenetic manipulation*

To inhibit $AC_{STR}$ neurons in the bilateral AC (Fig. 5), we delivered a continuous green light from the laser (5mW, 532nm, Shanghai Laser & Optics Century) during the stimulus period (-0.2 ~ 1s from the stimulus onsets) in 50% of trials. To suppress $M2_{\rightarrow AC}$ axon terminals in the right AC, we delivered a continuous green light from the laser (5 ~ 8mW, 532nm,

Shanghai Laser & Optics Century) starting 200ms before the stimulus presentation (-0.2 ~ 1 s from the stimulus onset). To control the effectiveness of laser light itself during optogenetic inhibition of the target neurons, we conducted control experiments delivering laser lights onto the dental cement.

**Video monitoring of orofacial and body movements of mice performing a task**

The data acquisition and analysis were performed as previously reported[84]. We used a camera (G3-GM11-M2020-Genie, Teledyne DALSA) and lens (TEC-M55 2/3" 55mm telecentric lens, C-Mount) to record left eye of task-performing animals at a high resolution (1200 x 800 pixels) by illuminating the left side of the animal's face with infrared light source (850 nm, S-IR5850, Skycares). We recorded images at 30 Hz using the Image Acquisition Toolbox provided by MATLAB.

We calculated the pupil size of the left eye of the task-performing mice using the following custom-written MATLAB code: 1) drawing an ROI that covers the left eye, 2) setting the optimal brightness threshold to determine the pupil boundary, 3) converting the ROI image to a binary image by filling in each pixel with the black and white values according to the threshold (*imbinarize*, built-in MATLAB function), 4) filling holes within the pupil boundary to avoid any artifacts from measuring pupil area due to light reflection on the cornea (*imfill*, built-in MATLAB function), 5) identifying a convex hull that includes the inside part of the pupil (*bwconvhull*, a built-in MATLAB function), and 6) counting the number of pixels within the convex hull as the pupil size across frames. We normalized the pupil size using the following equation, resulting in a number ranging from 0 (smallest size) to 1 (largest size):

$$Normalized\ Pupil(t) = (Pupil(t) - min(Pupil))/max(Pupil)$$

## *In vivo* calcium imaging experiments

*Data acquisition*

To avoid bleaching of calcium signals during the behavior task, we conducted an imaging experiment in a stationary or moving block one day and tested the other block the next day. Each imaging session was completed when mice showed three consecutive miss trials or when the imaging time reached one hour. We analyzed the same neurons tracked over two consecutive days in imaging data.

We performed an *in vivo* calcium imaging experiment using a miniature fluorescence microscope (Inscopix). Images were acquired at 20 frames per second (10 frames per second for $AC_{PPC}$ neurons) using nVista HD software (Inscopix). We cropped superfluous imaging areas that contained no neural signal. The LED power (0.2 ~ 0.5mW) and gain value (1 ~ 4) were adjusted based on the overall brightness of the GCaMP signals. For the simultaneous M2 axon activation and calcium imaging at the AC (Fig. 6g-k), we used the nVoke system (Inscopix) to acquire images at 10 frames per second alternating with 0.4mW of EX-LED light activation (red excitation light to activate ChrimsonR). The light delivery started 200ms before the stimulus onset and ended at the stimulation offset (-0.2 ~ 1s).

*Preprocessing of imaging data*

The acquired image data were processed with Inscopix Data Processing Software (IDPS, Inscopix). Images were downsampled by a factor of 4 and spatially filtered (highCutoff: 0.5; lowCutoff: 0.01 for PPC excitatory neurons; highCutoff: 0.5; lowCutoff: 0.005 for the other groups). Filtered images were corrected for lateral motion (IDPS implementation). Motion-corrected images were converted to ΔF/F images where F represents the average intensity of each pixel during the whole imaging time. Principal component analysis - independent component analysis (PCA-ICA) was used to identify cell boundaries on ΔF/F

images using IDPS implementation. We next extracted calcium signals by manually inspecting cell boundaries obtained from PCA-ICA on motion-corrected images and exported average intensities within cell boundaries. The same neurons were identified throughout several imaging sessions using longitudinal registration (IDPS implementation), and only neurons that appeared across imaging sessions were selected for further analysis.

*Calculation of response amplitudes and sorting neuronal type*

Exported calcium data were analyzed using custom MATLAB codes. The extracted calcium response data was converted to ΔF/F for each neuron. ΔF/F was calculated as $\Delta F/F = (F - F0)/F0$, where F0 represents the average fluorescence of a neuron across the imaging time. All the analyses were conducted based on the ΔF/F value.

To determine if a neuron responded to distinct stimuli (Fig. 2c), we compared average calcium activity during baseline (-0.2 ~ 0 s) and stimulation (0 ~ 1 s) periods using Wilcoxon signed-rank test ($P<0.01$, MATLAB implementation). The response amplitude for each trial was calculated by subtracting the average of baseline activity from the average of calcium activity during the first 1 s after stimulus onset. To dissect neuronal type (Fig. 2c), we compared Go and No-go responses if neurons showed significant responses to Go and No-go stimuli in one modality and classified as Go or No-go neurons if they had a significantly stronger response in the Go or No-go trials. Neurons that showed significant responses in one auditory and one visual stimulus were classified as “Dual,” while neurons with significant responses in three unisensory trial types were classified as “Triple.” “All” type neurons responded significantly in all unisensory trials. To examine how locomotion affects unisensory responses (Extended Data Fig. 2a), we compared the response amplitudes of each neuron from stationary and moving sessions using the Mann-Whitney U-test ($P < 0.01$).

To calculate the change in spontaneous activity of imaged neurons by locomotion onset and offset, we collected calcium activity and locomotion speed data at all locomotion onsets or offsets (-2 ~ 2s) and concatenated them. We then calculated the Pearson correlation coefficient between the two variables. We used the following conditions to define locomotion onsets and offsets during an imaging session.

Locomotion onset at 0 s must satisfy all of the following conditions:

1) *Average locomotion speed (-1 ~ -0.5 s) < 0.5cm/s;*

2) *Average locomotion speed (-0.5 ~ 1 s) < 0.5cm/s;*

*3) Average locomotion speed (0 ~ 250 ms) > 1cm/s;*

*4) Average locomotion speed (250 ~ 1000 ms) > 2cm/s;*

*5) No stimulus during -2 ~ 2 s.*

Locomotion offset at 0 s must satisfy all of the following conditions:

1) *Average locomotion speed (-1 ~ -0.5 s) > 2 cm/s;*

2) *Average locomotion speed (-0.5 ~ 1 s) > 1cm/s;*

*3) Average locomotion speed (0 ~ 250 ms) < 0.5cm/s;*

*4) Average locomotion speed (250 ~ 1000 ms) < 0.5cm/s;*

*5) No stimulus during -2 ~ 2 s.*

To calculate the change in $M2_{AC}$ activity at locomotion onset (Fig. 6f), we subtracted mean baseline activity (-1 ~ -0.5s from the locomotion onset) from mean calcium signal at early (0 ~ 1.5s from the locomotion onset) or late (3 ~ -1 from the locomotion offset) periods.

*Demixed principal component analysis of imaging data*

To visualize populational activity during the behavioral task over time, we used demixed principal component analysis (dPCA)[68]. The dPCA was performed using trial-averaged calcium activity aligned at stimulus onset (-1 ~ 3 s) of all neurons across the eight

unisensory trial types (visual hit, visual miss, visual CR, visual FA, auditory hit, auditory miss, auditory CR, and auditory FA). To denoise the calcium data, we temporally downsampled it (factor 2) and applied Gaussian smoothing with a window size of three bins. We excluded sessions that had fewer than three trials of lick or no-lick in the unisensory and incongruent trials. The encoding PCs from the dPCA were classified into stimulus-related, decision-related, stimulus-decision interaction-related, and independent axes. To show trajectories for each trial type in Fig. 2g, 3a, 3c, and Extended Data Fig. 5d,6d, we used dPCA results derived from the all imaged neurons. For all quantifications, we used the dPCA results from each imaging session. We projected the activities of the multisensory trials (congruent and incongruent trials) by using transformation vectors obtained from the dPCA with the unisensory trials.

To quantify the similarities between trial types, we calculated Euclidean distances between coordinates after the stimulus onset (0 ~ 1 s) in a subspace containing the top 3 sorted PCs (top 3 stimulus PCs explained the 62.8% variance of the data on average). To compare neural trajectories based on locomotion state, trial-averaged activities of unisensory trials from stationary, start-moving, and keep-moving trials were analyzed by dPCA. To distinguish between start-moving and keep-moving data in the moving sessions, we projected trial data into the encoding PC axes from the dPCA of each moving session. The Euclidean distance between two trajectories was calculated 1 s after the stimulus onset. Projection distance was measured as the Euclidean distance between 0 and 1 s following the stimulus onset.

*dPCA based classifiers*

For classifiers (Fig. 2 and Extended Data Fig. 3,5,6), we projected single-trial activity onto the top encoding PC axes and computed Euclidean distances between single trial data (only correct trials for unisensory classification) and trial-averaged trajectories of the unisensory trials (for unisensory classification) or incongruent trials (for incongruent

classification) at each time points. Each test trial was classified into a trial type of the trial-averaged trajectory that showed the smallest Euclidean distance from the test trial trajectory. If the test trajectory showed a very short projection in the PC axes, its distance to the center of the trajectories at the pre-stimulus time points was smaller than the distance to the trial-averaged trajectories at each time point. We counted it as incorrect classification.

To determine the significance of similarity with visual trajectories in determining dominant modality (Fig. 3e,f), we first projected the activities of individual unisensory trials onto the top three stimulus encoding PC axes and calculated the Euclidean distance between each trajectory and the trial-averaged target visual trajectory (target visual trajectory: $V_G$ for $A_{NG}V_G$ classification; $V_{NG}$ for $A_GV_{NG}$ classification). To calculate the distribution of individual visual trials, we used linear discriminant analysis (LDA) to determine an Euclidean distance threshold that distinguishes visual trials from other visual and auditory trials. Finally, we classified individual incongruent trials according to their Euclidean distance to the trial-averaged target visual trajectory, with each trial classified as a visual-dominant trial if its Euclidean distance was less than the threshold. To statistically compare classifier accuracies, we calculated mean classifier accuracy between 0.5 and 1s following stimulus onset, when the classifiers attained a peak of classification accuracy, and compared between groups.

**Histology and Immunohistochemistry**

We performed histology experiments to confirm imaging sites after *in vivo* calcium imaging, injection and expression sites of viral vectors, and anatomical circuit tracing data. Mice were anesthetized with avertin (2,2,2-Tribromoethanol (Sigma-Aldrich), 125-250mg/kg, intraperitoneally) and transcardially perfused with 15ml of PBS, followed by 4% paraformaldehyde (PFA, w/v in PBS). Brain samples were post-fixed for 4 hours in the PFA at 4°C, then washed 3 times with PBS for 10 minutes each. After washing, the brain samples

were immersed in a 30% sucrose solution (w/v in PBS) for 2-5 days. When the brain samples sank, they were embedded in optimal cutting temperature medium (Tissue-Tek O.C.T. Compound, Sakura Finetek) and rapidly froze at -80°C. Frozen brain samples were sectioned into 40μm or 20μm (for immunostaining) in a coronal direction using a cryocut (Leica). We washed brain slices 3 times in PBS for 10 minutes before mounting them with an anti-bleaching mounting medium containing 4′,6-diamidino-2-phenylindole (DAPI) (Vector Labs). To immunostain the CaMKIIα, we permeabilized the brain sections for 30 min with 0.5% w/v Triton X-100 in PBS, then blocked with 2% w/v normal goat serum (NGS) in PBS for 2 hours at room temperature. The samples were incubated at 4°C for 48 hours with mouse anti-CaMKIIα antibodies (ab22609, abcam, 1:250 dilution in 2% NGS). After treating the primary antibodies, we washed the samples 3 times in PBS for 10 minutes. We used Alexa Fluor 594 goat anti-mouse IgG (A11005, Invitrogen, 1:250 dilution in PBS) to stain CaMKIIα for 2 hours at room temperature. Following that, we washed the samples in PBS 3 times for 10 minutes before mounting them with anti-bleaching medium with DAPI. Fluorescent images of brain slices were taken using a slide scanner (Zeiss Axio Scan. Z1) or a confocal microscope (Nikon A1 HD25).

**Statistical analysis**

We analyzed the data using custom-written codes in MATLAB (Mathworks). All data were presented as mean ± SEM unless otherwise noted. ‘N’ denotes the number of mice or sessions, whereas ‘n’ represents the number of neurons. All statistical analyses were described in the figure legends. All the statistical significances of the datasets were indicated as NS (not significant; $P \geq 0.05$), * ($P < 0.05$), ** ($P < 0.01$), *** ($P < 0.001$), and **** ($P < 0.0001$).

## References


1 Stein, B. E. *The new handbook of multisensory processing*. (MIT Press, 2012).

2 Gielen, S. C., Schmidt, R. A. & Van den Heuvel, P. J. On the nature of intersensory facilitation of reaction time. *Percept Psychophys* **34**, 161-168 (1983). https://doi.org/10.3758/bf03211343

3 Diederich, A. & Colonius, H. Bimodal and trimodal multisensory enhancement: effects of stimulus onset and intensity on reaction time. *Percept Psychophys* **66**, 1388-1404 (2004). https://doi.org/10.3758/bf03195006

4 Raposo, D., Sheppard, J. P., Schrater, P. R. & Churchland, A. K. Multisensory decision-making in rats and humans. *J Neurosci* **32**, 3726-3735 (2012). https://doi.org/10.1523/JNEUROSCI.4998-11.2012

5 Meijer, G. T., Pie, J. L., Dolman, T. L., Pennartz, C. M. A. & Lansink, C. S. Audiovisual Integration Enhances Stimulus Detection Performance in Mice. *Front Behav Neurosci* **12**, 231 (2018). https://doi.org/10.3389/fnbeh.2018.00231

6 Colavita, F. B. Human Sensory Dominance. *Perception & Psychophysics* **16**, 409-412 (1974). https://doi.org/Doi 10.3758/Bf03203962

7 McGurk, H. & MacDonald, J. Hearing lips and seeing voices. *Nature* **264**, 746-748 (1976). https://doi.org/10.1038/264746a0

8 Battaglia, P. W., Jacobs, R. A. & Aslin, R. N. Bayesian integration of visual and auditory signals for spatial localization. *J Opt Soc Am A Opt Image Sci Vis* **20**, 1391-1397 (2003). https://doi.org/10.1364/josaa.20.001391

9 Alais, D. & Burr, D. The ventriloquist effect results from near-optimal bimodal integration. *Curr Biol* **14**, 257-262 (2004). https://doi.org/10.1016/j.cub.2004.01.029

10 Fetsch, C. R., Turner, A. H., DeAngelis, G. C. & Angelaki, D. E. Dynamic reweighting of visual and vestibular cues during self-motion perception. *J Neurosci* **29**, 15601-15612 (2009). https://doi.org/10.1523/JNEUROSCI.2574-09.2009

11 Fetsch, C. R., Pouget, A., DeAngelis, G. C. & Angelaki, D. E. Neural correlates of reliability-based cue weighting during multisensory integration. *Nat Neurosci* **15**, 146-154 (2011). https://doi.org/10.1038/nn.2983

12 Song, Y. H. *et al.* A Neural Circuit for Auditory Dominance over Visual Perception. *Neuron* **93**, 940-+ (2017). https://doi.org/10.1016/j.neuron.2017.01.006

13 Choi, I. & Lee, S. H. Reduced activity of parvalbumin-positive interneurons in the posterior parietal cortex causes visually dominant multisensory decisions in freely navigating mice. *Mol Brain* **15**, 82 (2022). https://doi.org/10.1186/s13041-022-00968-x

14 Ernst, M. O. & Banks, M. S. Humans integrate visual and haptic information in a statistically optimal fashion. *Nature* **415**, 429-433 (2002). https://doi.org/10.1038/415429a

15 Kording, K. P. & Wolpert, D. M. Bayesian integration in sensorimotor learning. *Nature* **427**, 244-247 (2004). https://doi.org/10.1038/nature02169

16 Coen, P., Sit, T. P. H., Wells, M. J., Carandini, M. & Harris, K. D. Mouse frontal cortex mediates additive multisensory decisions. *Neuron* **111**, 2432-2447 e2413 (2023). https://doi.org/10.1016/j.neuron.2023.05.008

17 Keil, J., Muller, N., Ihssen, N. & Weisz, N. On the variability of the McGurk effect: audiovisual integration depends on prestimulus brain states. *Cereb Cortex* **22**, 221-231 (2012). https://doi.org/10.1093/cercor/bhr125

18 Jiang, W., Jiang, H. & Stein, B. E. Two corticotectal areas facilitate multisensory orientation behavior. *J Cogn Neurosci* **14**, 1240-1255 (2002). https://doi.org/10.1162/089892902760807230

19 Avillac, M., Ben Hamed, S. & Duhamel, J. R. Multisensory integration in the ventral intraparietal area of the macaque monkey. *J Neurosci* **27**, 1922-1932 (2007). https://doi.org/10.1523/JNEUROSCI.2646-06.2007

20 Mallick, D. B., Magnotti, J. F. & Beauchamp, M. S. Variability and stability in the McGurk effect: contributions of participants, stimuli, time, and response type. *Psychon Bull Rev* **22**, 1299-1307 (2015). https://doi.org/10.3758/s13423-015-0817-4

21 Sinnett, S., Spence, C. & Soto-Faraco, S. Visual dominance and attention: the Colavita effect revisited. *Percept Psychophys* **69**, 673-686 (2007). https://doi.org/10.3758/bf03193770

22 Crochet, S., Lee, S. H. & Petersen, C. C. H. Neural Circuits for Goal-Directed Sensorimotor Transformations. *Trends Neurosci* **42**, 66-77 (2019). https://doi.org/10.1016/j.tins.2018.08.011

23 Esmaeili, V. *et al.* Rapid suppression and sustained activation of distinct cortical regions for a delayed sensory-triggered motor response. *Neuron* **109**, 2183-2201 e2189 (2021). https://doi.org/10.1016/j.neuron.2021.05.005

24 Choi, I., Lee, J. Y. & Lee, S. H. Bottom-up and top-down modulation of multisensory integration. *Curr Opin Neurobiol* **52**, 115-122 (2018). https://doi.org/10.1016/j.conb.2018.05.002

25 McGinley, M. J. *et al.* Waking State: Rapid Variations Modulate Neural and Behavioral Responses. *Neuron* **87**, 1143-1161 (2015). https://doi.org/10.1016/j.neuron.2015.09.012

26 Ayaz, A., Saleem, A. B., Scholvinck, M. L. & Carandini, M. Locomotion controls spatial integration in mouse visual cortex. *Curr Biol* **23**, 890-894 (2013). https://doi.org/10.1016/j.cub.2013.04.012

27 Bennett, C., Arroyo, S. & Hestrin, S. Subthreshold Mechanisms Underlying State-Dependent Modulation of Visual Responses. *Neuron* **80**, 350-357 (2013). https://doi.org/10.1016/j.neuron.2013.08.007

28 Dipoppa, M. *et al.* Vision and Locomotion Shape the Interactions between Neuron Types in Mouse Visual Cortex. *Neuron* **98**, 602-+ (2018). https://doi.org/10.1016/j.neuron.2018.03.037

29 Fu, Y. *et al.* A Cortical Circuit for Gain Control by Behavioral State. *Cell* **156**, 1139-1152 (2014). https://doi.org/10.1016/j.cell.2014.01.050

30 Lee, A. M. *et al.* Identification of a Brainstem Circuit Regulating Visual Cortical State in Parallel with Locomotion. *Neuron* **83**, 455-466 (2014). https://doi.org/10.1016/j.neuron.2014.06.031

31 Niell, C. M. & Stryker, M. P. Modulation of Visual Responses by Behavioral State in Mouse Visual Cortex. *Neuron* **65**, 472-479 (2010). https://doi.org/10.1016/j.neuron.2010.01.033

32 Paken, J. M. P. *et al.* Behavioral-state modulation of inhibition is context-dependent and cell type specific in mouse visual cortex. *Elife* **5** (2016). https://doi.org/ARTNe14985
10.7554/eLife.14985

33 Polack, P. O., Friedman, J. & Golshani, P. Cellular mechanisms of brain state-dependent gain modulation in visual cortex. *Nature Neuroscience* **16**, 1331-U1227 (2013). https://doi.org/10.1038/nn.3464

34 Vinck, M., Batista-Brito, R., Knoblich, U. & Cardin, J. A. Arousal and Locomotion Make Distinct Contributions to Cortical Activity Patterns and Visual Encoding. *Neuron* **86**, 740-754 (2015). https://doi.org/10.1016/j.neuron.2015.03.028

35 McGinley, M. J., David, S. V. & McCormick, D. A. Cortical Membrane Potential Signature of Optimal States for Sensory Signal Detection. *Neuron* **87**, 179-192 (2015). https://doi.org/10.1016/j.neuron.2015.05.038

36 Zhou, M. *et al.* Scaling down of balanced excitation and inhibition by active behavioral states in auditory cortex. *Nature Neuroscience* **17**, 841-850 (2014). https://doi.org/10.1038/nn.3701

37 Nelson, A. *et al.* A Circuit for Motor Cortical Modulation of Auditory Cortical Activity. *Journal of Neuroscience* **33**, 14342-+ (2013). https://doi.org/10.1523/Jneurosci.2275-13.2013

38 Schneider, D. M., Nelson, A. & Mooney, R. A synaptic and circuit basis for corollary discharge in the auditory cortex. *Nature* **513**, 189-+ (2014). https://doi.org/10.1038/nature13724

39 Schneider, D. M., Sundararajan, J. & Mooney, R. A cortical filter that learns to suppress the acoustic consequences of movement. *Nature* **561**, 391-+ (2018). https://doi.org/10.1038/s41586-018-0520-5

40 Runyan, C. A., Piasini, E., Panzeri, S. & Harvey, C. D. Distinct timescales of population coding across cortex. *Nature* **548**, 92-96 (2017). https://doi.org/10.1038/nature23020

41 Williamson, R. S., Hancock, K. E., Shinn-Cunningham, B. G. & Polley, D. B. Locomotion and Task Demands Differentially Modulate Thalamic Audiovisual Processing during Active Search. *Curr Biol* **25**, 1885-1891 (2015). https://doi.org/10.1016/j.cub.2015.05.045

42 Zhou, Y. & Freedman, D. J. Posterior parietal cortex plays a causal role in perceptual and categorical decisions. *Science* **365**, 180-185 (2019). https://doi.org/10.1126/science.aaw8347

43 Lyamzin, D. & Benucci, A. The mouse posterior parietal cortex: Anatomy and functions. *Neurosci Res* **140**, 14-22 (2019). https://doi.org/10.1016/j.neures.2018.10.008

44 Freedman, D. J. & Ibos, G. An Integrative Framework for Sensory, Motor, and Cognitive Functions of the Posterior Parietal Cortex. *Neuron* **97**, 1219-1234 (2018). https://doi.org/10.1016/j.neuron.2018.01.044

45 Goard, M. J., Pho, G. N., Woodson, J. & Sur, M. Distinct roles of visual, parietal, and frontal motor cortices in memory-guided sensorimotor decisions. *Elife* **5** (2016). https://doi.org/10.7554/eLife.13764

46 Pho, G. N., Goard, M. J., Woodson, J., Crawford, B. & Sur, M. Task-dependent representations of stimulus and choice in mouse parietal cortex. *Nat Commun* **9**, 2596 (2018). https://doi.org/10.1038/s41467-018-05012-y

47 Nikbakht, N., Tafreshiha, A., Zoccolan, D. & Diamond, M. E. Supralinear and Supramodal Integration of Visual and Tactile Signals in Rats: Psychophysics and Neuronal Mechanisms. *Neuron* **97**, 626-639 e628 (2018). https://doi.org/10.1016/j.neuron.2018.01.003

48 Oude Lohuis, M. N., Marchesi, P., Pennartz, C. M. A. & Olcese, U. Functional (ir)relevance of posterior parietal cortex during audiovisual change detection. *J Neurosci* **42**, 5229-5245 (2022). https://doi.org/10.1523/JNEUROSCI.2150-21.2022

49 Harvey, C. D., Coen, P. & Tank, D. W. Choice-specific sequences in parietal cortex during a virtual-navigation decision task. *Nature* **484**, 62-68 (2012). https://doi.org/10.1038/nature10918

50 Raposo, D., Kaufman, M. T. & Churchland, A. K. A category-free neural population supports evolving demands during decision-making. *Nature Neuroscience* **17**, 1784-1792 (2014). https://doi.org/10.1038/nn.3865

51 Licata, A. M. *et al.* Posterior Parietal Cortex Guides Visual Decisions in Rats. *J Neurosci* **37**, 4954-4966 (2017). https://doi.org/10.1523/JNEUROSCI.0105-17.2017

52 Hwang, E. J., Dahlen, J. E., Mukundan, M. & Komiyama, T. History-based action selection bias in posterior parietal cortex. *Nat Commun* **8**, 1242 (2017). https://doi.org/10.1038/s41467-017-01356-z

53 Driscoll, L. N., Pettit, N. L., Minderer, M., Chettih, S. N. & Harvey, C. D. Dynamic Reorganization of Neuronal Activity Patterns in Parietal Cortex. *Cell* **170**, 986-999 e916 (2017). https://doi.org/10.1016/j.cell.2017.07.021

54 Tseng, S. Y., Chettih, S. N., Arlt, C., Barroso-Luque, R. & Harvey, C. D. Shared and specialized coding across posterior cortical areas for dynamic navigation decisions. *Neuron* **110**, 2484-2502 e2416 (2022). https://doi.org/10.1016/j.neuron.2022.05.012

55 Akrami, A., Kopec, C. D., Diamond, M. E. & Brody, C. D. Posterior parietal cortex represents sensory history and mediates its effects on behaviour. *Nature* **554**, 368-372 (2018). https://doi.org/10.1038/nature25510

56 Zhong, L. *et al.* Causal contributions of parietal cortex to perceptual decision-making during stimulus categorization. *Nat Neurosci* **22**, 963-973 (2019). https://doi.org/10.1038/s41593-019-0383-6

57 Gallero-Salas, Y. *et al.* Sensory and Behavioral Components of Neocortical Signal Flow in Discrimination Tasks with Short-Term Memory. *Neuron* **109**, 135-148 e136 (2021). https://doi.org/10.1016/j.neuron.2020.10.017

58 Yao, J. D., Gimoto, J., Constantinople, C. M. & Sanes, D. H. Parietal Cortex Is Required for the Integration of Acoustic Evidence. *Curr Biol* **30**, 3293-3303 e3294 (2020). https://doi.org/10.1016/j.cub.2020.06.017

59 Zingg, B. *et al.* Neural networks of the mouse neocortex. *Cell* **156**, 1096-1111 (2014). https://doi.org/10.1016/j.cell.2014.02.023

60 Zhang, S. *et al.* Organization of long-range inputs and outputs of frontal cortex for top-down control. *Nat Neurosci* **19**, 1733-1742 (2016). https://doi.org/10.1038/nn.4417

61 Lewis, J. W. & Van Essen, D. C. Corticocortical connections of visual, sensorimotor, and multimodal processing areas in the parietal lobe of the macaque monkey. *J Comp Neurol* **428**, 112-137 (2000). https://doi.org/10.1002/1096-9861(20001204)428:1<112::aid-cne8>3.0.co;2-9

62 Driver, J. & Noesselt, T. Multisensory interplay reveals crossmodal influences on 'sensory-specific' brain regions, neural responses, and judgments. *Neuron* **57**, 11-23 (2008). https://doi.org/10.1016/j.neuron.2007.12.013

63 Schlack, A., Sterbing-D'Angelo, S. J., Hartung, K., Hoffmann, K. P. & Bremmer, F. Multisensory space representations in the macaque ventral intraparietal area. *J Neurosci* **25**, 4616-4625 (2005). https://doi.org/10.1523/JNEUROSCI.0455-05.2005

64 Olcese, U., Iurilli, G. & Medini, P. Cellular and synaptic architecture of multisensory integration in the mouse neocortex. *Neuron* **79**, 579-593 (2013). https://doi.org/10.1016/j.neuron.2013.06.010

65 Wallace, M. T., Ramachandran, R. & Stein, B. E. A revised view of sensory cortical parcellation. *Proc Natl Acad Sci U S A* **101**, 2167-2172 (2004). https://doi.org/10.1073/pnas.0305697101

66 Shimaoka, D., Harris, K. D. & Carandini, M. Effects of Arousal on Mouse Sensory Cortex Depend on Modality (vol 22, pg 3160, 2018). *Cell Reports* **25**, 3230-3230 (2018). https://doi.org/10.1016/j.celrep.2018.11.105

67 Schneider, D. M. & Mooney, R. Motor-related signals in the auditory system for listening and learning. *Curr Opin Neurobiol* **33**, 78-84 (2015). https://doi.org/10.1016/j.conb.2015.03.004

68 Kobak, D. *et al.* Demixed principal component analysis of neural population data. *Elife* **5** (2016). https://doi.org/10.7554/eLife.10989

69 Chen, L., Wang, X. X., Ge, S. Y. & Xiong, Q. J. Medial geniculate body and primary auditory cortex differentially contribute to striatal sound representations. *Nature Communications* **10** (2019). https://doi.org/ARTN 418
10.1038/s41467-019-08350-7

70 Guo, L., Walker, W. I., Ponvert, N. D., Penix, P. L. & Jaramillo, S. Stable representation of sounds in the posterior striatum during flexible auditory decisions. *Nature Communications* **9** (2018). https://doi.org/ARTN 1534
10.1038/s41467-018-03994-3

71 Xiong, Q. J., Znamenskiy, P. & Zador, A. M. Selective corticostriatal plasticity during acquisition of an auditory discrimination task. *Nature* **521**, 348-+ (2015). https://doi.org/10.1038/nature14225

72 Ponvert, N. D. & Jaramillo, S. Auditory Thalamostriatal and Corticostriatal Pathways Convey Complementary Information about Sound Features. *Journal of Neuroscience* **39**, 271-280 (2019). https://doi.org/10.1523/Jneurosci.1188-18.2018

73 Lin, P. A., Asinof, S. K., Edwards, N. J. & Isaacson, J. S. Arousal regulates frequency tuning in primary auditory cortex. *Proc Natl Acad Sci U S A* **116**, 25304-25310 (2019). https://doi.org/10.1073/pnas.1911383116

74 Welch, R. B. & Warren, D. H. Immediate perceptual response to intersensory discrepancy. *Psychol Bull* **88**, 638-667 (1980).

75 Repp, B. H. & Penel, A. Auditory dominance in temporal processing: New evidence from synchronization with simultaneous visual and auditory sequences. *J Exp Psychol Human* **28**, 1085-1099 (2002). https://doi.org/10.1037//0096-1523.28.5.1085

76 Crapse, T. B. & Sommer, M. A. Corollary discharge across the animal kingdom. *Nat Rev Neurosci* **9**, 587-600 (2008). https://doi.org/10.1038/nrn2457

77 Matin, E. Saccadic suppression: a review and an analysis. *Psychol Bull* **81**, 899-917 (1974). https://doi.org/10.1037/h0037368

78 Bremmer, F., Kubischik, M., Hoffmann, K. P. & Krekelberg, B. Neural dynamics of saccadic suppression. *J Neurosci* **29**, 12374-12383 (2009). https://doi.org/10.1523/JNEUROSCI.2908-09.2009

79 Kuan, A. T. *et al.* Synaptic wiring motifs in posterior parietal cortex support decision-making. *bioRxiv*, 2022.2004.2013.488176 (2022). https://doi.org/10.1101/2022.04.13.488176

80 Romanski, L. M. Representation and integration of auditory and visual stimuli in the primate ventral lateral prefrontal cortex. *Cereb Cortex* **17 Suppl 1**, i61-69 (2007). https://doi.org/10.1093/cercor/bhm099

81 Calvert, G. A., Campbell, R. & Brammer, M. J. Evidence from functional magnetic resonance imaging of crossmodal binding in the human heteromodal cortex. *Curr Biol* **10**, 649-657 (2000). https://doi.org/10.1016/s0960-9822(00)00513-3

82 Siniscalchi, M. J., Phoumthipphavong, V., Ali, F., Lozano, M. & Kwan, A. C. Fast and slow transitions in frontal ensemble activity during flexible sensorimotor behavior. *Nat Neurosci* **19**, 1234-1242 (2016). https://doi.org/10.1038/nn.4342

83 Gulati, S., Cao, V. Y. & Otte, S. Multi-layer Cortical Ca2+ Imaging in Freely Moving Mice with Prism Probes and Miniaturized Fluorescence Microscopy. *Jove-J Vis Exp* (2017). https://doi.org/ARTN e55579
10.3791/55579

84 Kim, J. H., Ma, D. H., Jung, E., Choi, I. & Lee, S. H. Gated feedforward inhibition in the frontal cortex releases goal-directed action. *Nat Neurosci* **24**, 1452-1464 (2021). https://doi.org/10.1038/s41593-021-00910-9

## Main figures and legends

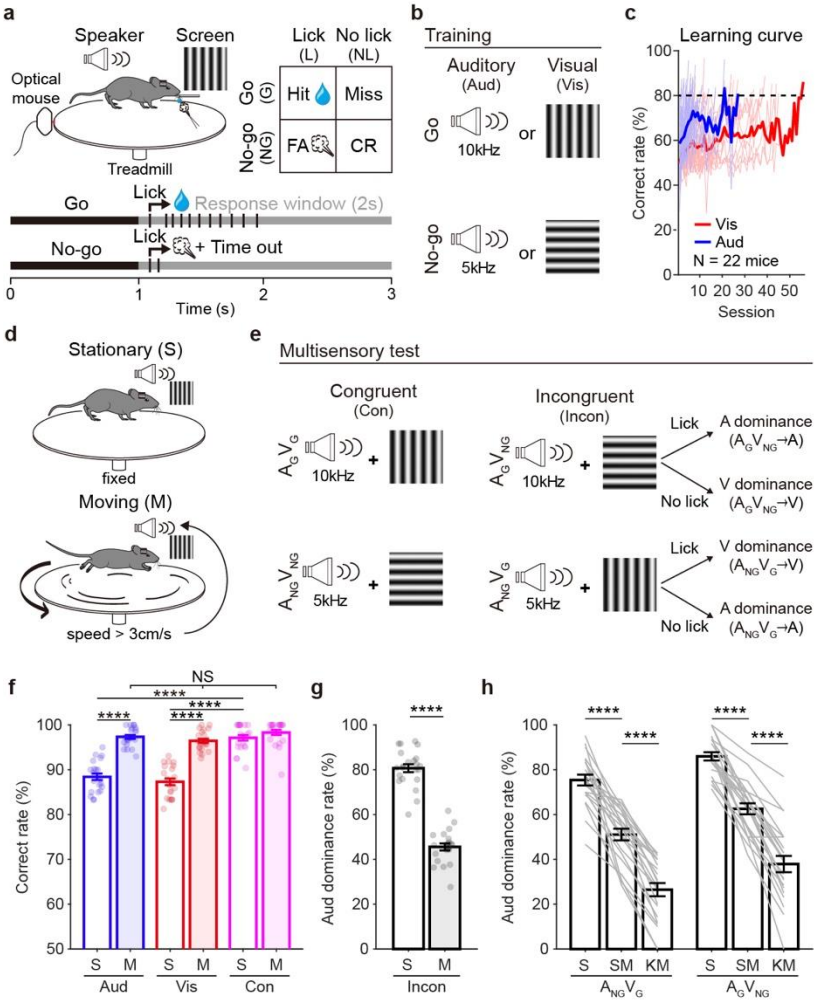


**Fig. 1 | Locomotion switches auditory-dominant decisions to visually dominant ones in mice under audiovisual conflicts**

**a**, Schematic illustration of the audiovisual discrimination task in a head-fixed mouse on the treadmill. G, go; NG, no-go; L, lick; NL, no lick; FA, false alarm; CR, correct rejection.

**b**, Stimuli used for behavioral training. Aud, auditory stimuli; Vis, visual stimuli.

**c**, Learning curves across mice trained with the task (N = 22 mice). Thin lines represent individual mice. The black dashed line indicates a criterion for expert performance (80% correct rate). Red, visual discrimination performance; Blue, auditory discrimination performance.

**d**, Schematics of stationary (top, S) and moving (bottom, M) conditions.

**e**, Audiovisual stimuli used for the multisensory test. Note that letter ‘A’ and ‘V’ after the arrow marks indicates auditory dominance and visual dominance respectively.

**f**, Correct rates of mice in the auditory (Aud), visual (Vis), and congruent (Con) trials (N = 22 mice). Each circle indicates one mouse. S, stationary; M, moving. Two-way ANOVA with Tukey’s test. Locomotion, $P < 0.0001$; Stimulus, $P < 0.0001$; Interaction: $P < 0.0001$.

**g**, Auditory dominance rates in the incongruent trials (Incon) (N = 22 mice). Note that auditory dominance rates were calculated as the fraction of incongruent trials when mice showed decisions following auditory Go/No-go rules. Wilcoxon signed-rank test.

**h**, Auditory dominance rates in the incongruent trials at different locomotion states (N = 22 mice). S, stationary; SM, start-moving; KM, keep-moving. Gray lines represent individual mouse data. Wilcoxon signed-rank test.

Data are presented as means ± SEM. *$P < 0.05$, **$P < 0.01$, ***$P < 0.001$, ****$P < 0.0001$;

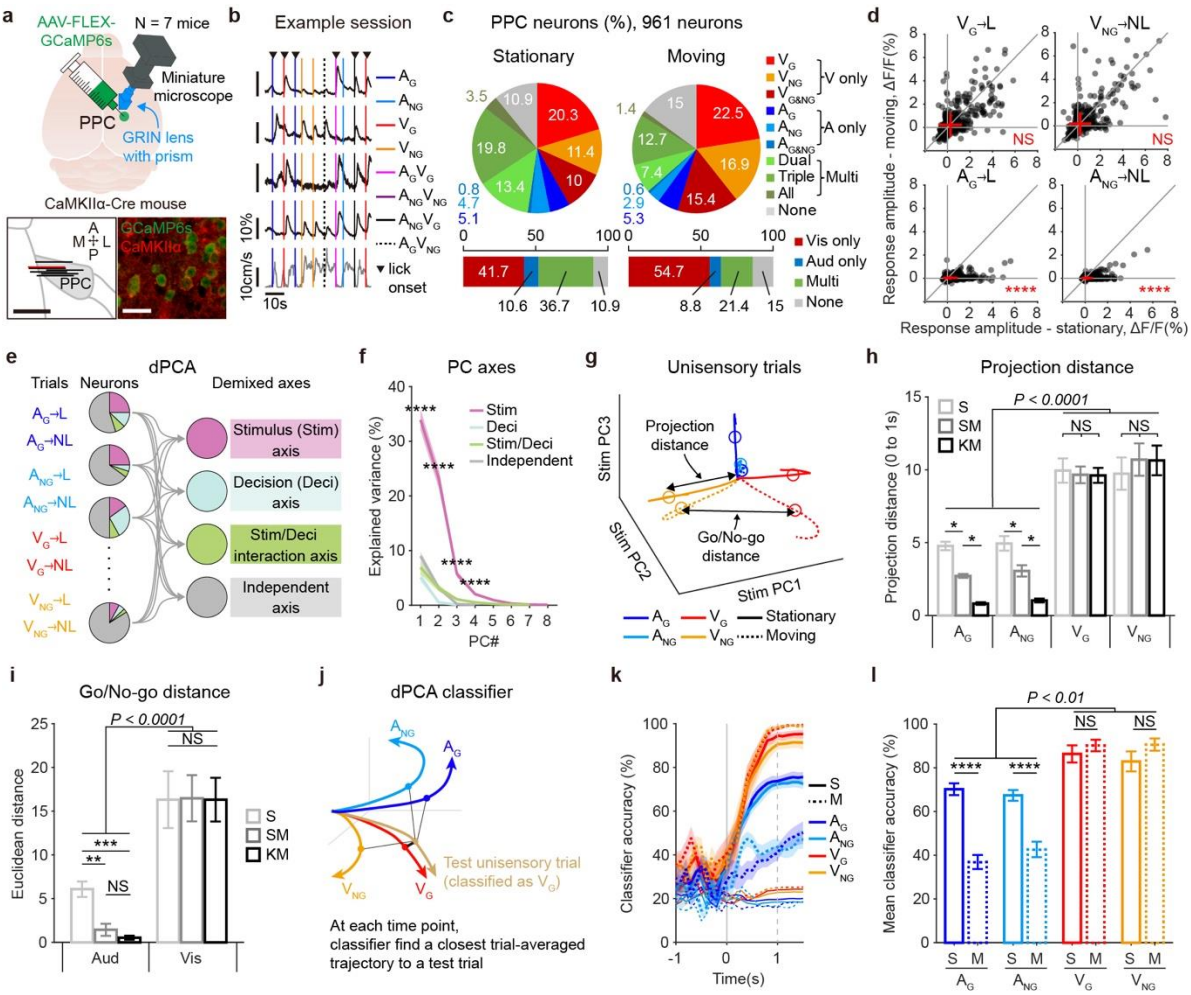


**Fig. 2 | Locomotion suppresses auditory representation while preserving visual representation in the PPC.**

**a**, Top, schematics of *in vivo* calcium imaging of the PPC excitatory neurons in a task-performing mouse. Bottom left, lens-inserted sites across the imaged mice (scale bar: 1mm); bottom right, immunohistochemical confirmation of CaMKIIα expression in GCaMP6s-expressing neurons (scale bars: 20 μm). 10 imaging experiments (10 stationary + 10 moving sessions) from 7 mice.

**b**, Measured calcium activities of 4 example neurons (black lines) and the locomotion speed (gray line) of an example moving mouse.

**c**, Response types of the PPC neurons (n = 961 neurons) in the stationary (left) and moving (right) conditions. Top, percentages of neurons classified according to the response types. Bottom, percentages of unisensory and multisensory neurons.

**d**, Stimulus-evoked response amplitudes of the PPC excitatory neurons (n = 961) in the correct unisensory trials at different locomotion states. Dots indicate individual neurons. Red cross lines indicate means ± standard deviations. Red, paired-sample t-test between response amplitudes at stationary and moving conditions.

**e**, Schematic illustration of dPCA to decompose the PPC populational activity into demixed axes representing specific task-relevant variables. Stim, stimulus; Deci, decision.

**f**, Percentages of explained variances of top 20 demixed PCs calculated in 10 stationary and 10 moving sessions (N = 20). Lines with shades are means ± SEM. Asterisks indicate statistical comparisons between the stimulus PCs and other PCs. One-way ANOVA with Fisher's LSD test.

**g**, Stimulus PC trajectories averaged across unisensory correct trials from all stationary or moving sessions. Circles indicate 1 s after the stimulus onset. Projection distance indicates the Euclidean distance between the points at 0 s and 1 s after the stimulus onset. Go/No-go distance indicates the Euclidean distance between Go and No-go trajectories at 1 s after the stimulus onset.

**h**, Projection distances of the unisensory trajectories at different states (N = 10). Two-way ANOVA with Fisher's LSD test. Stimulus, $P < 0.0001$; Locomotion, $P = 0.00085$; Interaction: $P = 0.0029$.

**i**, Go/No-go distances in the auditory (Aud) or visual (Vis) trials at different states (N = 10). Two-way ANOVA with Fisher's LSD test. Stimulus, $P < 0.0001$; Locomotion, $P = 0.039$; Interaction, $P = 0.034$.

**j**, Schematic illustration of the dPCA classifier that predicts trial types based on the Euclidean distance between a test trial trajectory and trial-averaged trajectories in the same subspace.

**k**, Accuracies of the dPCA classifier in sorting unisensory trial types. Solid lines, mean accuracies in stationary sessions; Dashed lines, mean accuracies in moving sessions; Thin lines, upper boundaries of 95% confidence intervals with shuffled trial labels. Colors, unisensory trial types. Vertical gray lines, stimulus onset (solid) and offset (dashed).

**l**, Mean classifier accuracies during the 0.5 – 1s period after the stimulus onset (N = 10). Two-way ANOVA with Fisher's LSD test. Stimulus, $P < 0.0001$; Locomotion, $P < 0.0001$; Interaction, $P < 0.0001$.

Data are presented as means ± SEM except for **d**. NS (not significant); *$P < 0.05$, **$P < 0.01$, ***$P < 0.001$, ****$P < 0.0001$.

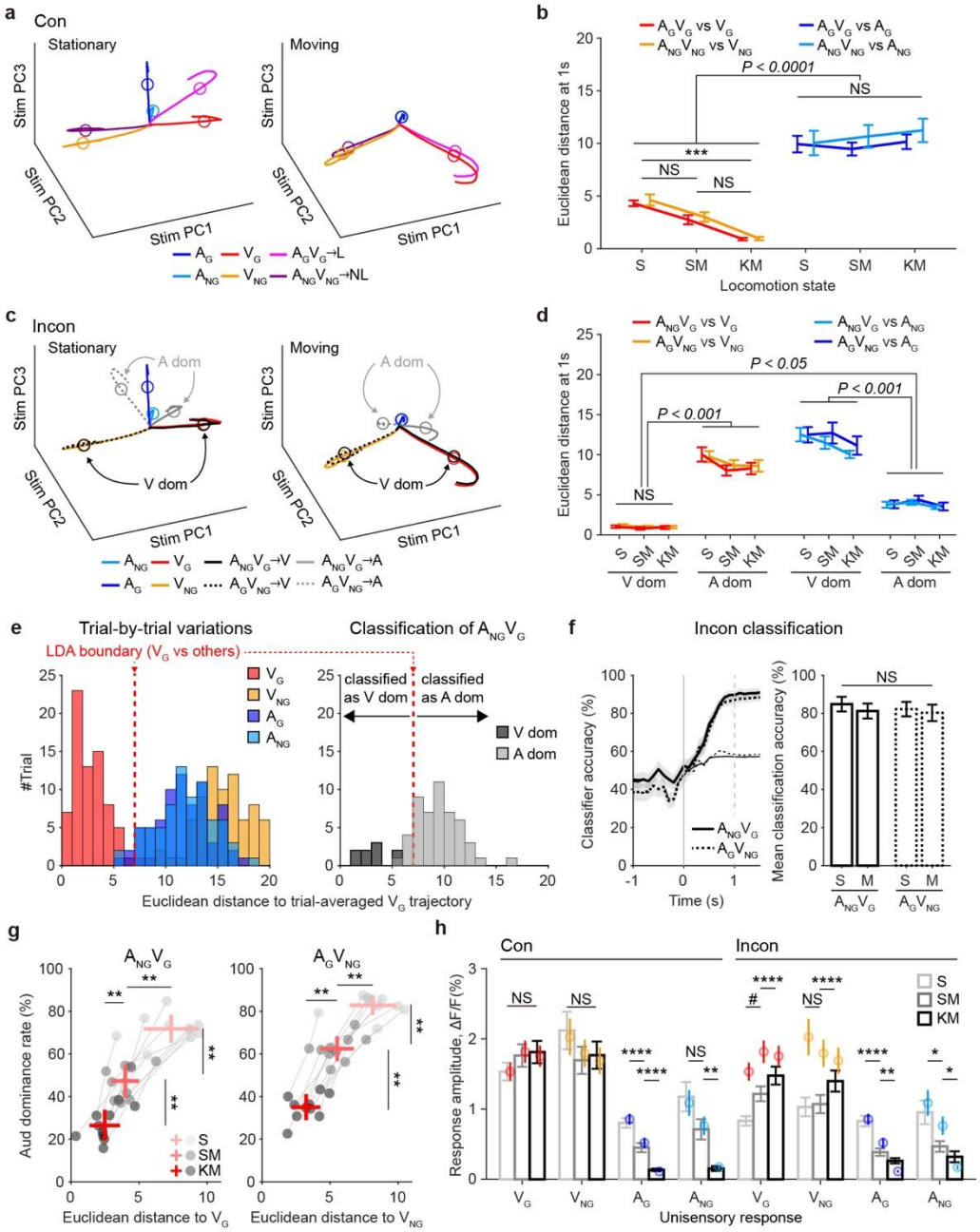


**Fig. 3 | The similarity between visual and multisensory representations in the PPC predicts dominant modality in multisensory decisions.**

**a**, Trajectories of trial-averaged calcium traces across all sessions for congruent and unisensory trials in the stimulus subspace from stationary (left) and moving (right) trials.

**b**, Mean Euclidean distances between congruent and unisensory trajectories for 1s during stimulus presentation at different locomotion states (N = 10). Two-way ANOVA with Fisher's LSD test. Pair type, $P < 0.0001$; Locomotion, $P = 0.022$; Interaction, $P = 0.0068$.

**c**, Same as **a**, but for incongruent and unisensory trials. Note that the incongruent trajectories were similar to the visual trajectories when mice made visual-dominant decisions. Black lines, trajectories for visual-dominant trials; Gray lines, trajectories for auditory-dominant trials. Solid lines, for $A_{NG}V_G$ trials; Dashed lines, for $A_GV_{NG}$ trials.

**d**, Same as **b**, but between incongruent and unisensory trajectories (N = 10). Two-way ANOVA with Fisher's LSD test. Pair type, $P < 0.0001$; Locomotion, $P = 0.014$; Interaction, $P = 0.64$.

**e**, Left, an example session data showing Euclidean distances between individual unisensory trajectories and the trial-averaged $V_G$ trajectory at 1s after the stimulus onset. Note that the LDA boundaries were set at the distance where $V_G$ trials were separated from other trials the most. Right, Euclidean distances between individual $A_{NG}V_G$ trajectories and the trial-averaged $V_G$ trajectory. LDA boundary was used to classify the dominant modality in $A_{NG}V_G$ trials. Dark gray, visual-dominant trials; light gray, auditory-dominant trials.

**f**, Left, accuracies of the LDA classifier in predicting dominance of multisensory trials (N = 10). Solid lines for $A_{NG}V_G$ trials; Dashed lines for $A_GV_{NG}$ trials; Thin gray lines, upper boundaries of 95% confidence intervals with shuffled trial labels. Vertical gray lines, stimulus onset (solid) and offset (dashed). Right, mean classifier accuracy at 1s after the stimulus onset (N = 10). S, stationary state; M, moving state. One-way ANOVA, $P = 0.93$.

**g**, Euclidean distances from the incongruent trials to the visual trajectory and the auditory dominance rates of mice at different locomotion states (N = 10). Left, $A_{NG}V_G$ trials; right, $A_GV_{NG}$ trials. Dots connected by gray lines, data from individual imaging. Red crosses, means ± standard deviations. Wilcoxon signed-rank test.

**h**, Response amplitudes of unisensory-responsive neurons to congruent and incongruent stimuli at different locomotion states. Circles with error bars indicate response amplitudes of the same neurons in unisensory visual (red) and auditory (blue) trials. Mann-Whitney U test

(between S and SM or KM) and Wilcoxon signed-rank test (between SM and KM) with Bonferonni correction (multiplied by 3) on the multisensory responses.

Data are presented as means ± SEM except for **g**. NS (not significant); #$P < 0.1$, *$P < 0.05$, **$P < 0.01$, ***$P < 0.001$, ****$P < 0.0001$.

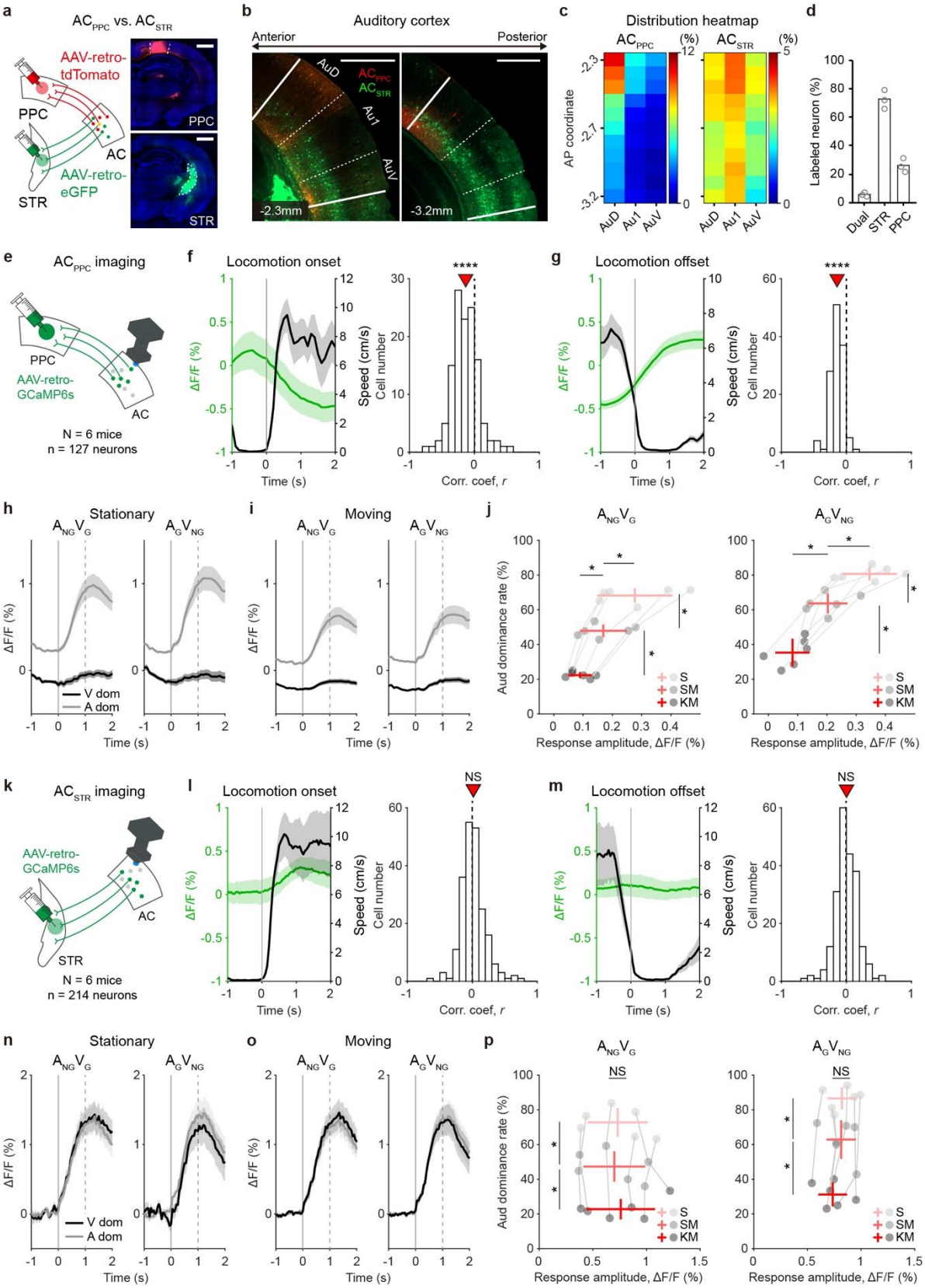


**Fig. 4 | Locomotion preferentially suppresses auditory outputs to the parietal cortex.**

**a**, Schematic illustration (left) and injection sites (right) of retrograde AAVs for dual retrograde tracing of the AC neurons that project to the PPC (red, $AC_{PPC}$) and to the posterior STR (green, $AC_{STR}$). Scale bars, 1 mm.

**b**, Representative images showing $AC_{PPC}$ and $AC_{STR}$ neurons at the anterior (left, -2.3mm from the bregma) and the posterior (right, -3.2mm from the bregma) AC. White lines, boundaries of the AC; White dashed lines, boundaries between AC subareas. Scale bars, 500 μm.

**c**, Heatmaps representing percentages of labeled $AC_{PPC}$ neurons (left) or $AC_{STR}$ neurons (right) in each subregion of the AC at different anterior-posterior coordinates.

**d**, Percentages of labeled neurons in the AC. Circles, data from individual brain samples.

**e**, Schematic illustration of *in vivo* calcium imaging of the $AC_{PPC}$ neurons. 127 neurons were imaged from 6 mice.

**f**, Left, mean calcium traces of $AC_{PPC}$ neurons (green) and mean locomotion speeds of mice (black) aligned to the locomotion onset. Right, distribution of Pearson correlation coefficients between locomotion speeds and calcium activities of individual neurons at locomotion onsets. The red triangle represents the mean correlation coefficients across all neurons. A vertical dotted line indicates zero. Wilcoxon signed-rank test.

**g**, Same for **f**, but for the locomotion offset. Wilcoxon signed-rank test.

**h**, Calcium activities of $AC_{PPC}$ neurons in the incongruent trials at stationary state. Black line and shades, for visual-dominat trials; Gray line and shades, for auditory-dominant trials. Calcium activities between the two dominant trials were significantly different at every time points ($P < 0.0001$). Wilcoxon signed-rank test.

**i**, Same for **h**, but for moving state. Calcium activities between the two dominant trials were significantly different at every time points ($P < 0.0001$). Wilcoxon signed-rank test.

**j**, Mean response amplitudes of $AC_{PPC}$ neurons and auditory dominance rates of mice in $A_{NG}V_{G}$ (left) and $A_{G}V_{NG}$ (right) trials at different locomotion states (N = 6). Dots connected with gray

lines, individual mice data. Red crosses, means ± standard deviations. Wilcoxon signed-rank test.

**k**-**p**, Same as **e**-**j**, but for the $AC_{STR}$ neurons (214 neurons from 6 mice).

Data are presented as means ± SEM except for **j**,**p**. NS (not significant), *$P < 0.05$, ****$P < 0.0001$.

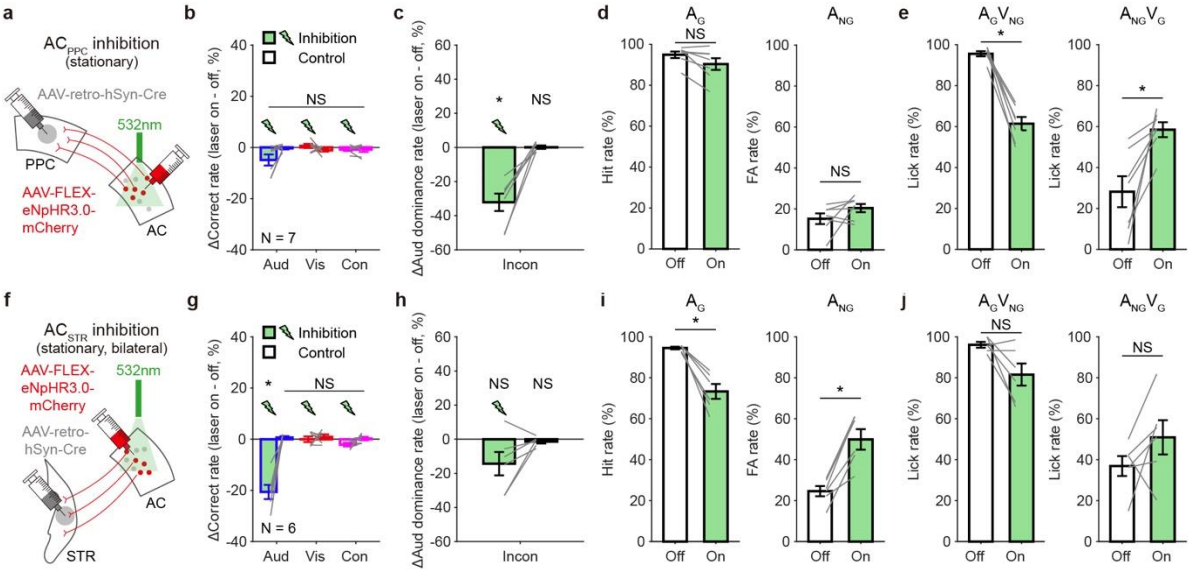


**Fig. 5 | Double dissociation of AC$_{PPC}$ and AC$_{STR}$ neurons in perceptual decision-making.**

**a**, Schematic for optogenetic inhibition of the AC$_{PPC}$ neurons in stationary mice performing audiovisual discrimination task.

**b**, Performance changes by optogenetic inactivation of the AC$_{PPC}$ neurons in the auditory, visual, and congruent trials (N = 7 mice). Gray lines, individual mice. Inhibition, sessions with light on the AC; Control, sessions with light on the dental cement. Wilcoxon signed-rank test for each data.

**c,** Changes in auditory-dominant rates by AC$_{PPC}$ inactivation in the incongruent trials. Wilcoxon signed-rank test for each data.

**d,** Changes in Hit and FA rates by AC$_{PPC}$ inactivation in the auditory trials from the inhibition sessions. Off, laser off trial; On, laser on trial. Wilcoxon signed-rank test.

**e**, Changes in lick rates by AC$_{PPC}$ inactivation in the incongruent trials from the inhibition sessions. Wilcoxon signed-rank test.

**f-j**, Same as **a-e**, but for optogenetic inactivation of the AC$_{STR}$ neurons (N = 6 mice).

Gray lines, individual mice; Bars, means ± SEM. Statistical comparisons with zero were indicated above individual bars. NS (non-significant), *$P$ < 0.05.

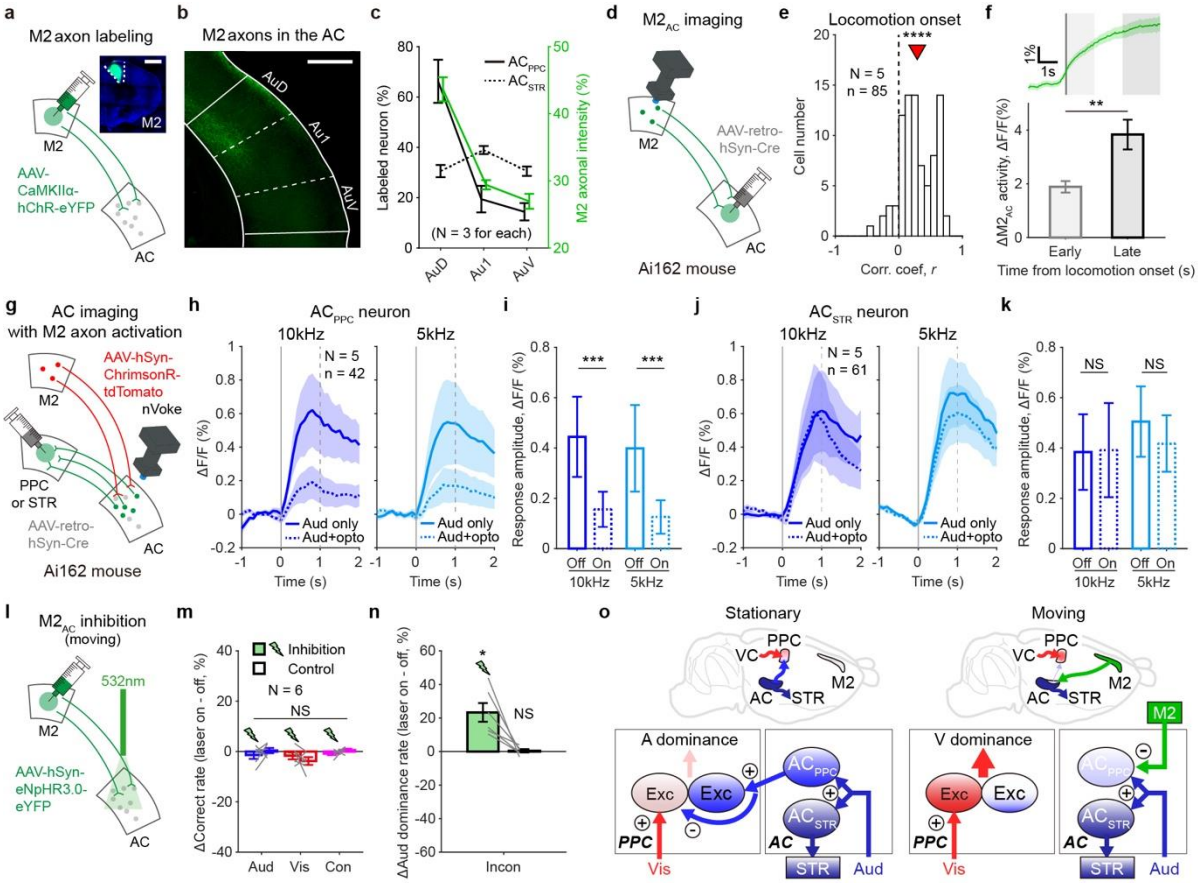


**Fig. 6 | M2-to-AC projection inhibits $AC_{PPC}$ neurons and induces visually dominant decisions during locomotion.**

**a**, Schematic illustration of anterograde labeling M2 axons in the AC. Inset, an example coronal brain slice showing virus injection site at M2. Scale bar, 1 mm.

**b**, A representative image of virus-expressing M2 axons in the subregions of anterior AC. Scale bar, 500 μm.

**c**, Percentages of the number of labeled neurons (black) and the intensity of M2 axons (green) in the subregions of anterior AC. Solid line, $AC_{PPC}$ neurons; dotted line, $AC_{STR}$ neurons.

**d**, Schematic illustration of *in vivo* calcium imaging of $M2_{AC}$ neurons.

**e**, Distribution of Pearson correlation coefficients between calcium activities and locomotion onsets across individual $M2_{AC}$ neurons. 85 neurons from 5 mice. Wilcoxon signed-rank test.

**f**, Top, mean activity of $M2_{AC}$ neurons after locomotion onsets. A gray vertical line, locomotion onset; lighter gray shade, early locomotion period (0 – 1.5 s from the onset); darker gray shade, late locomotion period (> 3s from the onset). Bottom, mean activities of $M2_{AC}$ neurons in the early and late locomotion periods. Wilcoxon signed-rank test.

**g**, Schematic illustration of *in vivo* calcium imaging of the projection-specific AC neurons together with optogenetic activation of M2 axons in the AC using the nVoke system.

**h**,**i**, Average calcium traces (**h**) and mean response amplitudes (**i**) of the $AC_{PPC}$ neurons (42 neurons from 5 mice) in response to the 10kHz (left) and 5kHz (right) pure tones with (dotted) or without (solid) optogenetic activation of the M2 axons. Wilcoxon signed-rank test.

**j**,**k**, Same as **h**,**i**, but for the $AC_{STR}$ neurons (61 neurons from 5 mice). Wilcoxon signed-rank test.

**l**, Schematic illustration of optogenetic inhibition of the M2 axons in the AC in task-performing mice at moving states.

**m**, Performance changes by optogenetic inhibition of the M2 axon in the AC during the auditory, visual, and congruent trials (N = 6 mice). Gray lines, individual mice. Inhibition, sessions with light on the AC; Control, sessions with light on the dental cement. Wilcoxon signed-rank test for each data.

**n**, Changes in auditory dominance rates by the M2 axon inhibition in the AC during the incongruent trials. Wilcoxon signed-rank test for each data.

**o**, Summary illustration of the brain areas interacting with each other to resolve audiovisual conflicts and make multisensory decisions at different locomotion states.

Data are presented as means ± SEM. NS (not significant), $*P < 0.05$, $**P < 0.01$, $***P < 0.001$.

## Extended data figures and legends

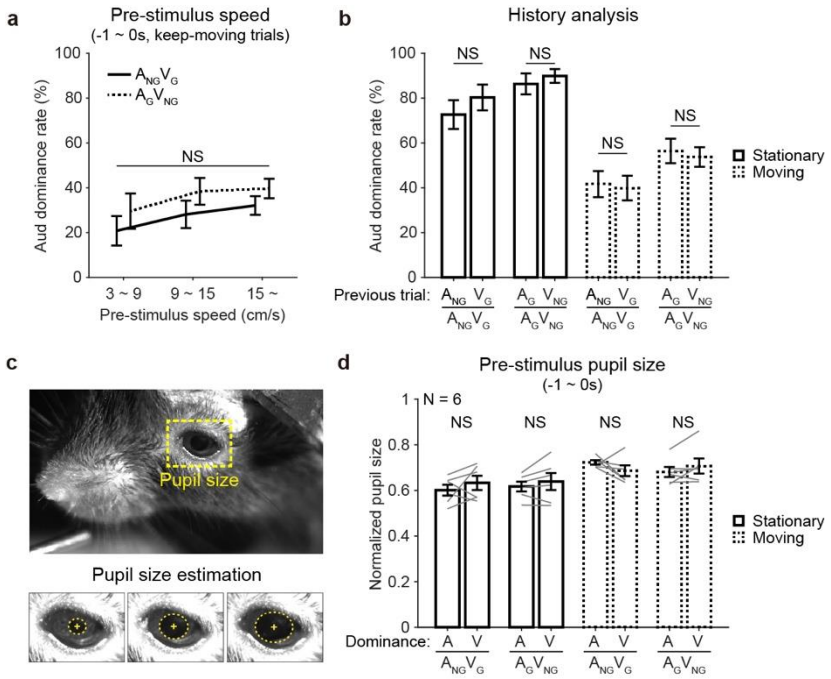


**Extended Data Fig. 1 | Analysis of the effects of pre-stimulus locomotion speeds, trial history, and pupil size on the auditory dominance rates.**

**a**, Auditory dominance rates at different pre-stimulus locomotion speeds in $A_{NG}V_{G}$ (gray solid line), $A_{G}V_{NG}$ (gray dashed line), and total incongruent trials (black) from the keep-moving state. One-way ANOVA with Fisher's LSD test.

**b**, Auditory dominance rates in incongruent trials after different types of unisensory trials. Gray lines indicate individual mice. Wilcoxon signed-rank test.

**c**, Example snapshot of a mouse head on the treadmill (top) and automatically estimated pupil boundaries at three different time points (bottom).

**d**, Mean pre-stimulus pupil sizes in the incongruent trials when mice showed auditory (A) or visual (V) dominance at different locomotion states (N = 6). Gray lines indicate individual mice. Data are presented as means ± SEM. NS (not significant).

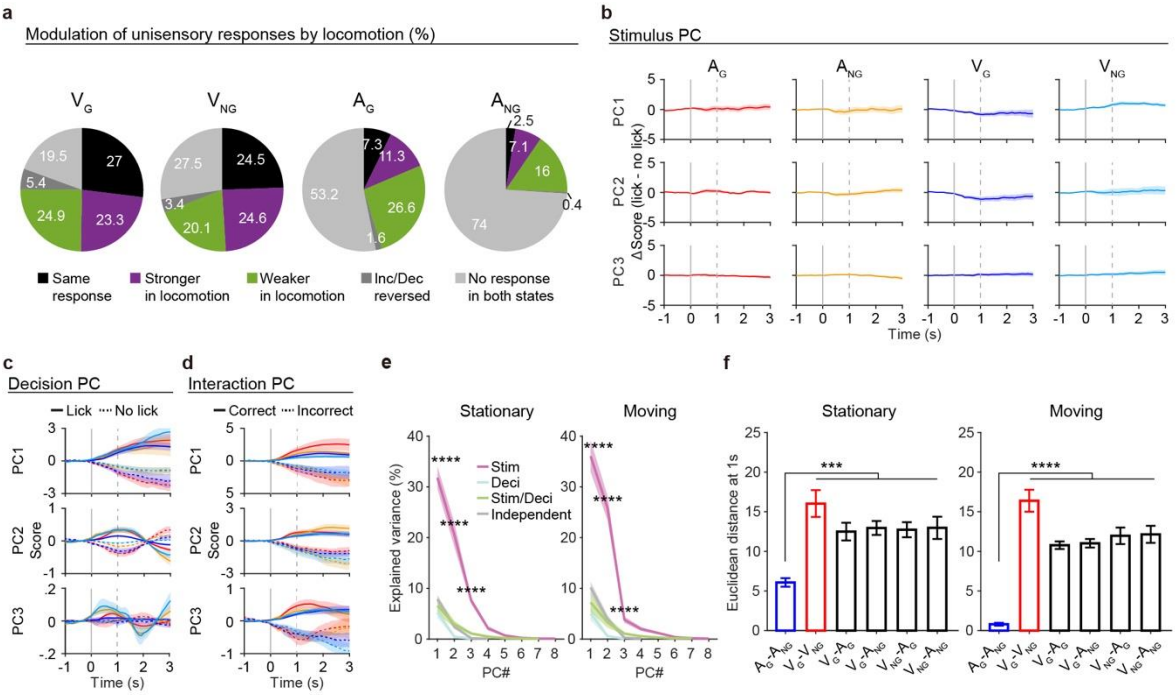


**Extended Data Fig. 2 | Unisensory response changes during locomotion and additional dPCA analysis of the PPC excitatory neurons.**

**a**, Changes in unisensory responses of the PPC excitatory neurons by locomotion.

**b**, Differences in the top 3 PC values in lick trials compared to no-lick trials in the stimulus PC axes after dPCA (N = 20). Note that the PCs in the stimulus axes were not different between lick and no-lick decisions of mice (Δ Score ≈ 0).

**c**, Comparisons of the top 3 PC values in the decision axes. Colors indicate unisensory types as shown in **d**. Note that decision PCs clearly dissect lick (solid line) and no-lick (dotted line) trials.

**d**, Same as **c**, but for the PCs in the interaction axes. Note that interaction PCs clearly dissect correct and incorrect trials

**e**, Percentage of explained variances of top 20 demixed PCs from dPCA of the stationary (left, N = 10) and the moving sessions (right, N = 10). Asterisks indicate statistical comparisons between the stimulus PCs and other PCs. One-way ANOVA with Fisher's LSD test.

**f**, Mean Euclidean distances in a pair of the unisensory trajectories in the stimulus subspace isolated from stationary (left, N = 10) and moving (right, N = 10) sessions. Note that the Euclidean distances are larger between visual Go and No-go trajectories than those between auditory Go and No-go trajectories in both conditions. One-way ANOVA with Fisher's LSD test.

Data are presented as means ± SEM. NS (not significant), ***$P < 0.001$; ****$P < 0.001$.

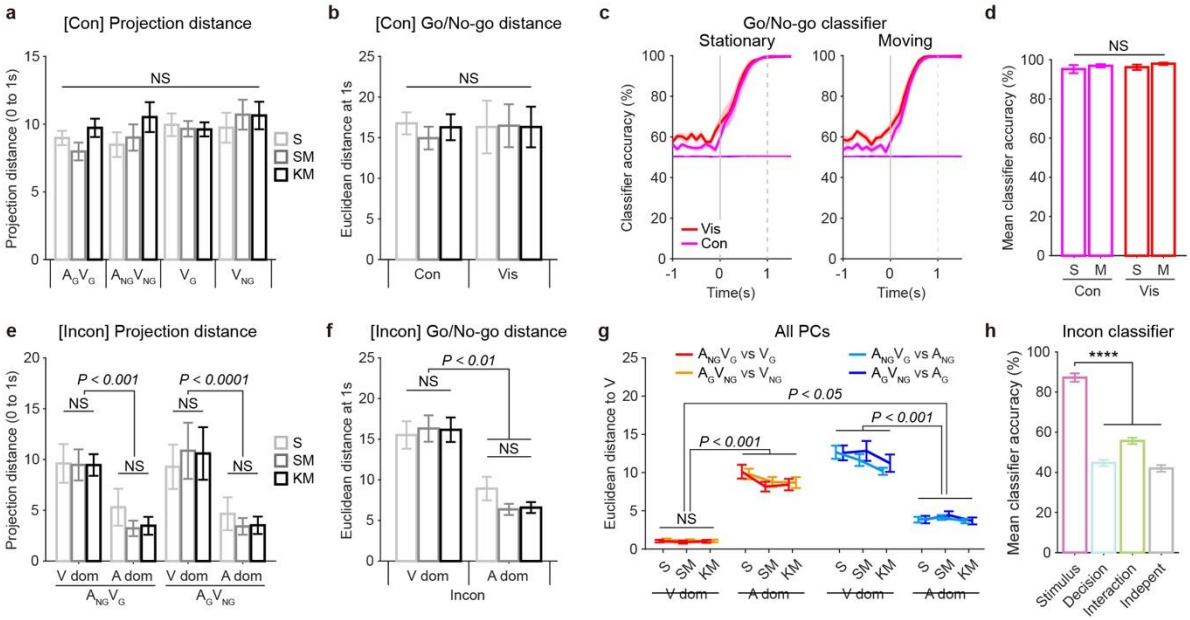


**Extended Data Fig. 3 | Additional dPCA results from the PPC neurons in the multisensory trials.**

**a**, Projection distances of neural trajectories in the stimulus subspace during congruent audiovisual and visual trials at different states (N = 10). One-way ANOVA, $P = 0.48$.

**b**, Euclidean distances between stimulus trajectories of Go and No-go trials (Go/No-go distances) in the congruent (Con) and visual (Vis) trials at different states (N = 10). One-way ANOVA, $P = 0.97$.

**c**, Classification accuracies of the visual Go and No-go trials and congruent Go and No-go trials in the stationary (left) and the moving (right) states (N = 10).

**d**, Mean Go/No-go classifier accuracies during the 0.5 – 1s period after the stimulus onset (N = 10). One-way ANOVA, $P = 0.53$.

**e**,**f**, Same as **a**,**b**, but for the incongruent audiovisual trials (N = 10). Note that the incongruent trials were sorted into visual-dominant and auditory-dominant trials. Two-way ANOVA with Fisher's LSD test. **e**, Trial type, $P < 0.0001$; Locomotion, $P = 0.61$; Interaction, $P = 0.28$. **f**, Dominance, $P < 0.0001$; Locomotion, $P = 0.076$; Interaction, $P = 0.39$.

**g**, Euclidean distances between the incongruent audiovisual trajectories and the unisensory visual or auditory trajectories of all PCs in the stimulus subspace (N = 10). Two-way ANOVA with Fisher's LSD test. Pair type, $P < 0.0001$; Locomotion, $P = 0.033$; Interaction, $P = 0.68$.

**h**, Mean classifier accuracies (N = 20) in identifying the four types of incongruent trials (two stimulus conditions with visual- or auditory-dominant decisions) by using neural trajectories in the stimulus, decision, interaction, and independent subspaces. One-way ANOVA with Fisher's LSD test.

Data are presented as means ± SEM. NS (not significant), *$P < 0.05$, **$P < 0.01$, ***$P < 0.001$, ****$P < 0.0001$.

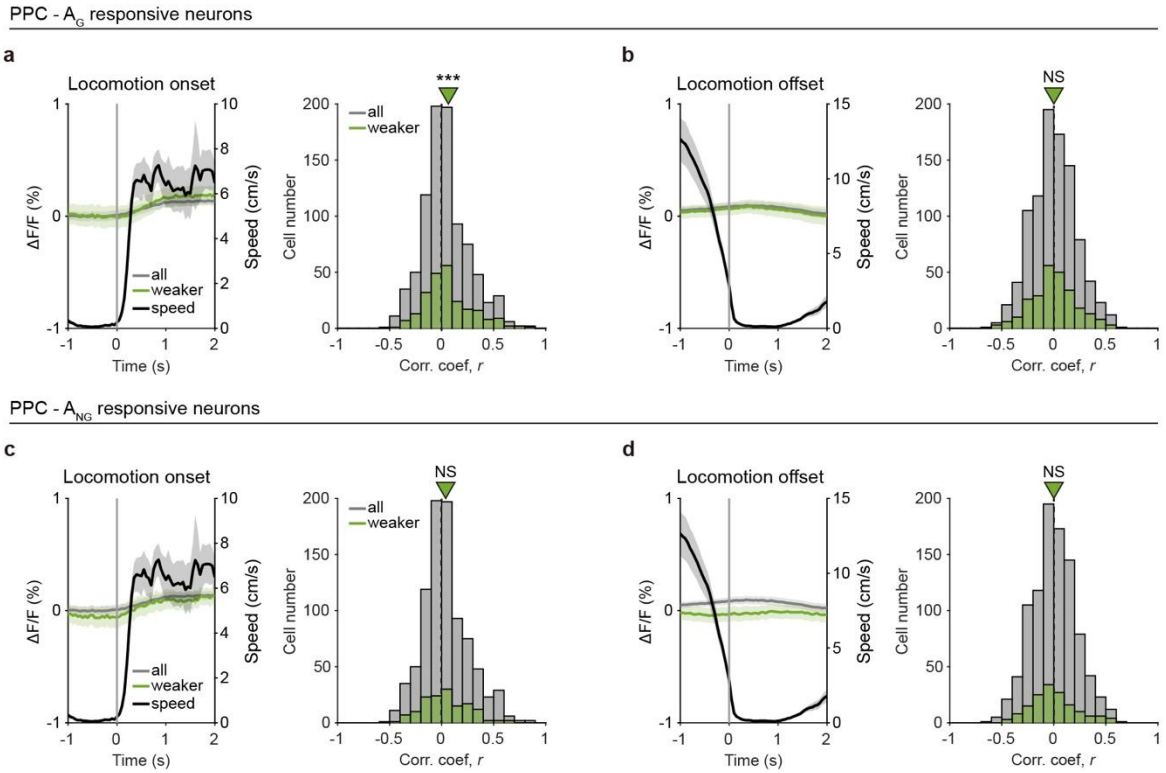


**Extended Data Fig. 4 | Locomotion-related activities in the PPC excitatory neurons.**

**a**, Left, the mean calcium trace of the $A_G$ neurons (green for $A_G$ neurons that showed weaker auditory responses during locomotion (as shown in Extended Data Fig. 2a); gray for all $A_G$ neurons) and the mean locomotion speed of mice (black) aligned to the locomotion onset. Right, a histogram of Pearson correlation coefficients between the activity changes in those neurons and the locomotion speeds during -2 ~ 2 s of the locomotion onset. Arrowheads, mean correlation coefficients. Wilcoxon signed-rank test.

**b**, Same as **a**, but for the locomotion offsets. Wilcoxon signed-rank test.

**c**,**d**, Same as **a**,**b**, but for the $A_{NG}$ neurons. Wilcoxon signed-rank test.

Traces with shades are means ± SEM. NS (not significant), ***$P < 0.001$.

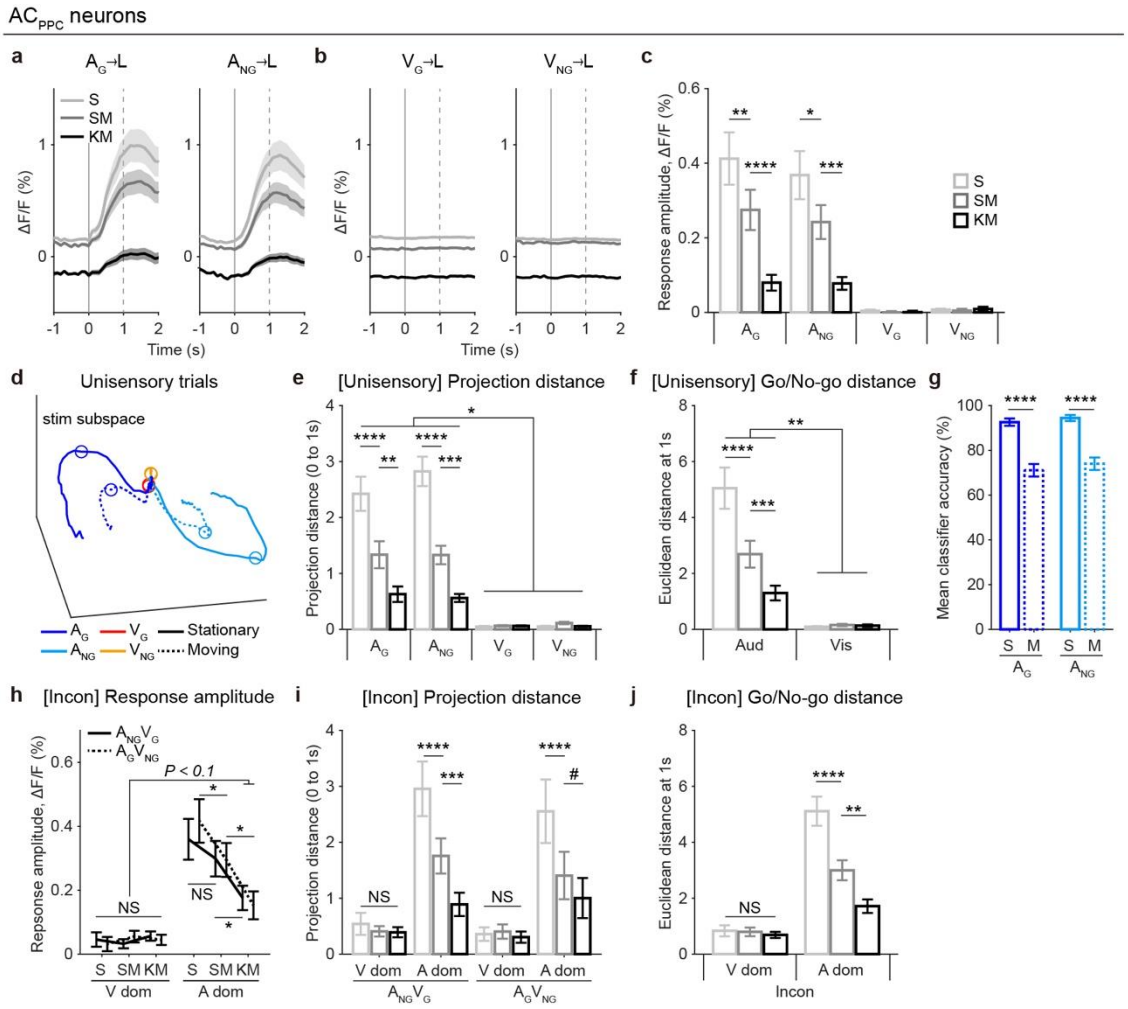


**Extended Data Fig. 5 | Neural activities of the $AC_{PPC}$ neurons at different locomotion states.**

**a**, Mean calcium traces of the $AC_{PPC}$ neurons (n = 127) in the trials with the $A_G$ stimulus (left) and with the $A_{NG}$ stimulus (right) at different locomotion states. Note that the responses were suppressed when mice showed longer locomotion.

**b**, Same as **a**, but for the $AC_{PPC}$ neurons in the trials with the $V_G$ (left) and $V_{NG}$ stimuli (right) at different locomotion states.

**c**, Mean response amplitudes of the $AC_{PPC}$ neurons (n = 127) in the unisensory trials at different locomotion states. Two-way ANOVA test with Fisher's LSD test. Stimulus, $P < 0.0001$; Locomotion, $P < 0.0001$; Interaction, $P < 0.0001$;

**d**, Neural trajectories of the $AC_{PPC}$ neurons in three PCs of the stimulus subspace from the dPCA. Four colors in trajectories represent unisensory trial types. Solid lines, stationary conditions; dotted lines, moving conditions.

**e**,**f**, Projections distances of the unisensory trajectories (**e**) and distances between Go and No-go trajectories (**f**) at different locomotion states (N = 6 for each data). Two-way ANOVA test with Fisher's LSD test. **e**, Stimulus, $P < 0.0001$; Locomotion, $P < 0.0001$; Interaction, $P < 0.0001$. **f**, Stimulus, $P < 0.0001$; Locomotion, $P < 0.0001$; Interaction, $P < 0.0001$;

**g**, Mean classifier accuracies of auditory stimuli classification (N = 6). Two-way ANOVA with Fisher's LSD test. Stimulus, $P < 0.0001$ ; Locomotion, $P < 0.0001$ ; Interaction, $P = 0.0009$.

**h**-**j**, Same as **c**,**e**,**f**, but for the incongruent trials (N = 6). Two-way ANOVA test with Fisher's LSD test. **h**, Trial type, $P < 0.0001$; Locomotion, $P < 0.0001$; Interaction, $P < 0.0001$. **i**, Trial type, $P < 0.0001$; Locomotion, $P < 0.0001$; Interaction, $P < 0.0001$. **j**, Dominance, $P < 0.0001$; Locomotion, $P < 0.0001$; Interaction, $P < 0.0001$.

Gray scales in lines and bars represent locomotion states. Light gray, stationary (S); dark gray, start-moving (SM); black, keep-moving (KM). Data are presented as means ± SEM. NS (not significant), #$P < 0.1$, *$P < 0.05$, **$P < 0.01$, ***$P < 0.001$, ****$P < 0.0001$.

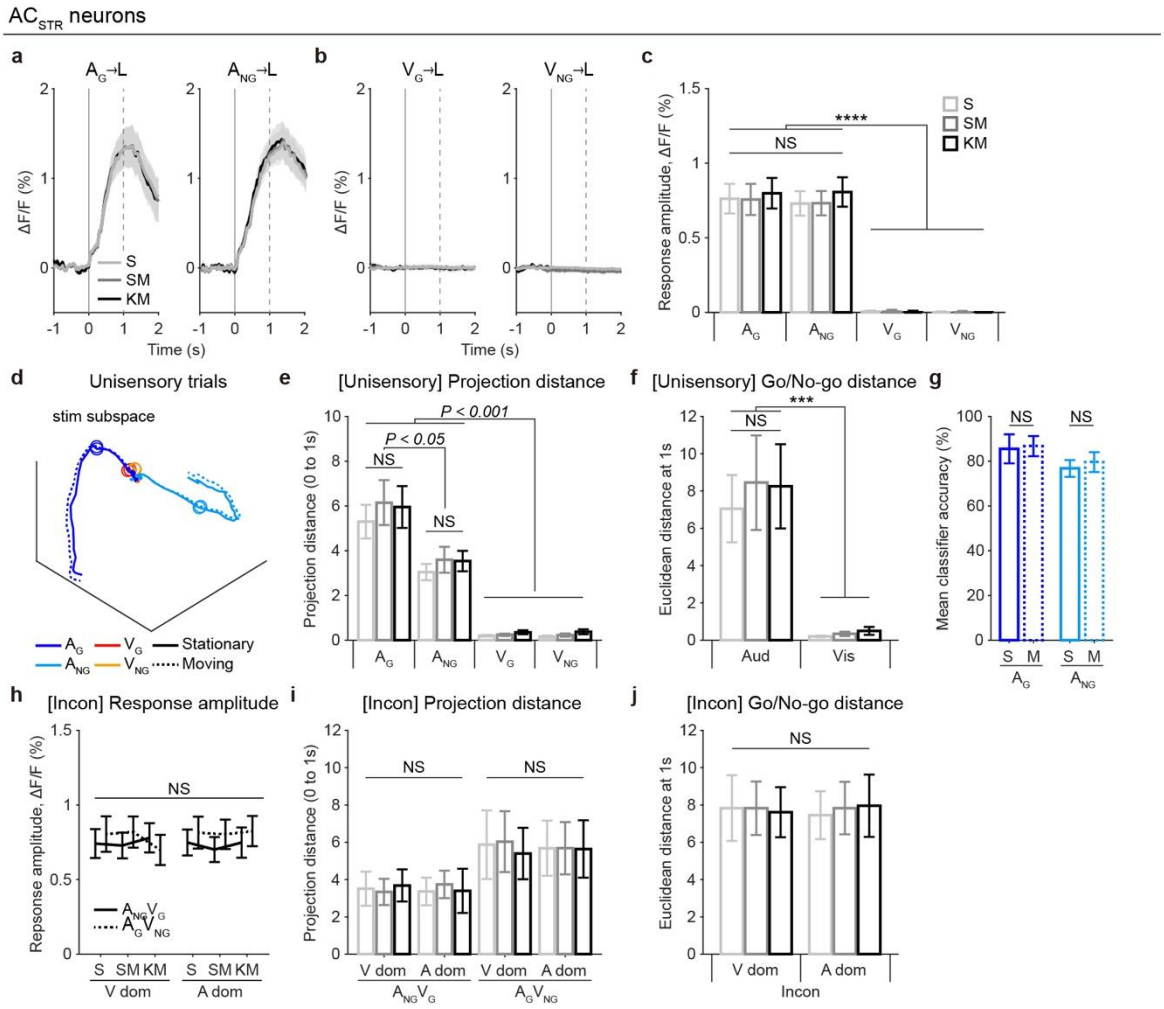


**Extended Data Fig. 6 | Neural activities of the $AC_{STR}$ neurons at different locomotion states.**

**a-j**, Same as Extended Data Fig. 5, but for the $AC_{STR}$ neurons.

**a**, Mean calcium traces of the $AC_{STR}$ neurons (n = 214) in the trials with the $A_G$ stimulus (left) and with the $A_{NG}$ stimulus (right) at different locomotion states.

**b**, Same as **a**, but for the $AC_{STR}$ neurons in the trials with the $V_G$ (left) and $V_{NG}$ stimuli (right) at different locomotion states.

**c**, Mean response amplitudes of the $AC_{STR}$ neurons (n = 214) in the unisensory trials at different locomotion states (n = 214 neurons). Two-way ANOVA test with Fisher's LSD test. Stimulus, $P < 0.0001$; Locomotion, $P = 0.87$; Interaction, $P = 0.99$;

**d**, Neural trajectories of the $AC_{STR}$ neurons in three PCs of the stimulus subspace from the dPCA. Four colors in trajectories represent unisensory trial types. Solid lines, stationary conditions; dotted lines, moving conditions.

**e**,**f**, Projections distances of the unisensory trajectories (**e**) and distances between Go and No-go trajectories (**f**) at different locomotion states (N = 6 for each data). Two-way ANOVA with Fisher's LSD test. **e**, Stimulus, $P < 0.0001$ ; Locomotion, $P = 0.49$; Interaction, $P = 0.99$. **f**, Stimulus, $P < 0.0001$ ; Locomotion, $P = 0.49$; Interaction, $P = 0.99$.

**g**, Mean classifier accuracies of auditory stimuli classification (N = 6). Two-way ANOVA with Fisher's LSD test. Stimulus, $P < 0.0001$ ; Locomotion, $P = 0.70$; Interaction, $P = 0.81$.

**h**-**j**, Same as **c**,**e**,**f**, but for the incongruent trials (N = 6). Two-way ANOVA test with Fisher's LSD test. **h**, Trial type, $P = 0.77$; Locomotion, $P = 0.97$; Interaction, $P = 0.98$. **i**, Trial type, $P < 0.0001$ ; Locomotion, $P = 0.94$; Interaction, $P = 0.99$. **j**, Dominance, $P = 0.99$ ; Locomotion, $P = 0.98$; Interaction, $P = 0.97$.

Gray scales in lines and bars represent locomotion states. Light gray, stationary (S); dark gray, start-moving (SM); black, keep-moving (KM). Data are presented as means ± SEM. NS (not significant), ****$P < 0.0001$.